Capacity Analysis of

Faster-Than-Nyquist MIMO Systems

MICHAEL JOHN YUHAS

Department of Electrical and Computer Engineering

McGill University

Montreal, Canada

April 2016

A thesis submitted to McGill University in partial fulfillment of the requirements of the degree of Master of Engineering.

Abstract

Demand for wireless data is expected to continue to increase in the coming decades. One of the driving factors behind this growth is the availability of mobile data via cellular networks. 4G and LTE technologies have enabled video streaming and other bandwidth intensive applications on mobile devices. It is expected that the fifth generation of mobile networks will need to supply enough capacity to support streaming of higher quality video from more devices than any previous network. Furthermore, the Internet of things will lead to an increase in transmission of data gathered from remote sensing devices across the network. 5G cellular must meet this demand for data while respecting spectrum bandwidth and power limitations. It is likely that 5G will turn to non-orthogonal modulation schemes to take full advantage of existing bandwidth.

This thesis explores two non-orthogonal modulation schemes that have the potential to appear in 5G networks. MIMO (Multiple Input Multiple Output) takes advantage of multiple transmit and receive antennas to generate extra spatial dimensions. These spatial dimensions allow a system to transmit more data in the same bandwidth with the same power constraints as a SISO (Single Input Single Output) system. Another scheme that will be explored is FTN (Faster Than Nyquist) signaling. FTN creates inter-symbol interference by compressing the transmitted symbols in the time domain. This compression does not lead to an increase in bandwidth, but does allow more data to be transmitted in a given amount of time. This thesis analyzes the channel capacity for both of these technologies independently and combined. Furthermore, alternative FTN receiver

architectures are explored and their capacities derived and compared to the traditional receiver architecture with channel state information known at the receiver and with channel state information known at the transmitter.

Sommaire

Il est prévu que la demande pour les données sans fil continuera d'augmenter dans les décennies à venir. Un des facteurs principaux de cette croissance est la disponibilité des données dans les réseaux cellulaires. Les technologies 4G et LTE ont rendu possible la vidéo en direct et autres applications qui exigent beaucoup de débit dans les appareils mobiles. Il est prévu que la cinquième génération des réseaux mobiles ait besoin de fournir une capacité suffisante pour fournir la vidéo en direct de plus haute qualité pour plus d'appareils que les réseaux précédents. De plus, l'Internet des objets causera une augmentation de transmission de données des capteurs sans fil. Les réseaux 5G doivent satisfaire cette demande de données tout en respectant les limitations de puissance et de bande passante. Il est probable que 5G se tournera vers la modulation non-orthogonale pour tirer profit de toute la bande passante existante.

Cette thèse explore deux solutions de modulation non-orthogonale qui ont le potentiel d'apparaître dans les réseaux 5G. MIMO (Multiple Input Multiple Output) tire avantage des antennes d'émetteur et récepteur additionnelles pour générer les dimensions spatiales supplémentaires. Ces dimensions permettent au système de transmettre plus de données sur la même bande passante et les mêmes contraintes de puissance qu'un système SISO (Single Input Single Output). L'autre approche étudiée est la signalisation FTN (Faster Than Nyquist). FTN crée de l'interférence inter-symbole en compressant les symboles transmis dans le domaine temporel. Cette compression ne cause pas une augmentation de bande passante, mais permet de transmettre plus de données dans un

intervalle de temps fixé. Cette thèse analyse la capacité du canal pour les deux technologies, séparément et combinées. De plus, des architectures alternatives pour récepteurs FTN sont explorées et leurs capacités sont dérivées et comparées à ceux d'un récepteur d'architecture traditionnelle avec l'information d'état du canal connue seulement à récepteur et seulement à transmetteur.

Acknowledgements

I would like to thank Dr. Jan Bajcsy, my supervisor, for teaching me the process of research and exposing me to a theoretical side of engineering that I did not know existed. Through his supervision I not only learned critical skills in academic research, but also about teaching and preparing the next generation of engineers for their lives in academia or industry.

I'd like to thank Yi Feng for helping me understand many mathematical concepts and also for giving me valuable feedback on the process of academic writing. I'd like to thank Dr. Yong Jin Daniel Kim for initially inspiring me to look more closely at Faster-than-Nyquist signaling and for listening to any ideas I had on the subject.

Lastly, I'd like to thank Mikael Arguedas for helping me to translate my abstract from English to French. He was also able to provide me with good insights on the applicability of my research.

Table of Contents

List of Figures

Preface

The research in this thesis has led to the conference paper: “On the Capacity of Faster-than-Nyquist MIMO Transmission with CSI at the Receiver” by Michael Yuhas, Yi Feng, and Dr. Jan Bajcsy [1]. The proposal for the paper was put forward by Michael Yuhas. This includes the idea to analyze the capacity of a combined FTN and MIMO communication system and the concept of the orthogonalized FTN MIMO receiver. Yi Feng derived the general form of the capacity formula that was used to calculate the capacity of both proposed architectures. Dr. Jan Bajcsy supervised the research and made corrections to the derived formulas as well as verifying that the results made sense and agreed with previous research in the field.

Chapter 1. Introduction

This chapter serves as an introduction to the current state of wireless communications and introduces FTN and MIMO technologies and their current role in wireless communications. The motivation for this thesis is shown to arise from the need for more capacity from a limited amount of channel bandwidth. It is important to note that capacity is a property of a communication channel and not of a system itself. A particular system can be designed to approach the maximum information rate of a channel, but can never exceed its capacity.

1.1. The Current State of Wireless Communications

Currently, there are many types of networks that facilitate wireless transmission of data: local area networks (LANs), personal area networks (PANs), and cellular networks. This section will focus on a popular protocol for each of these major network categories and demonstrate the increased availability and capacity of these networks that has led to the current state of wireless communications.

A LAN (Local Area Network) is a network that covers a limited area such as a building or small campus. Wi-Fi (IEEE 802.11) is a fairly ubiquitous standard for wireless LANs in North America and the world as whole. Wi-Fi was initially released in 1999 by a consortium of companies called the Wi-Fi alliance [2]. Today Wi-Fi is supported by many laptops and mobile phones and Wi-Fi access networks are often provided by institutions to their guests and clients. The advantage of Wi-Fi lies in the ubiquity of the standard and the decentralization of network control. Each deployed Wi-Fi network can

be managed independently and the controlling institution can provide Internet access to users under whatever conditions are desired [3]. This is also Wi-Fi's biggest disadvantage as it does not provide mobile users with an always connected access point governed by one method of billing and conditions [3]. Furthermore, Wi-Fi was not designed to accommodate users moving between networks and devices moving at high speeds [3].

Personal area networks are designed to network electronic devices between distances from a few centimeters to a few meters. This type of network is useful for connecting peripherals to personal devices such as smart phones, tablets, headsets, and various input devices. Bluetooth (IEEE 802.15.1) is a fairly ubiquitous protocol for PANs. Because of the distances involved, this protocol was designed to be low power with transmitting power between one and one hundred milliwatts [4]. Communication through a gateway allows information gathered by the Bluetooth sensor network to become available to any other Internet connected device. The advantages of Bluetooth lie in its low power short range networking capability, but the requirement of a dedicated gateway to achieve Internet access [4] provides a major obstacle for devices relying solely on Bluetooth protocols.

Cellular networks are a common Internet access method for mobile devices. Unlike LANs which are localized to a single building or cluster of buildings, cellular networks span entire nations. Cellular networks divide the coverage area into cells; within each cell a mobile device only communicates with that cell's base station [5]. The base station can route traffic within the cell or externally through wireless, wireline, or optical backhaul. The latest deployed cellular network protocol is LTE (Long Term Evolution). LTE can

provide mobile users with broadband mobile access anywhere in a cellular network where LTE hardware is installed although the actual speed of the broadband connection could vary considerably depending on network and link conditions [6]. The network's size guarantees that access is available even in rural areas where public Wi-Fi networks would not be available. The downside of LTE is limited connection speeds. The next generations of mobile networks, however, is expected to remedy this condition and provide a unified access scheme for mobile devices.

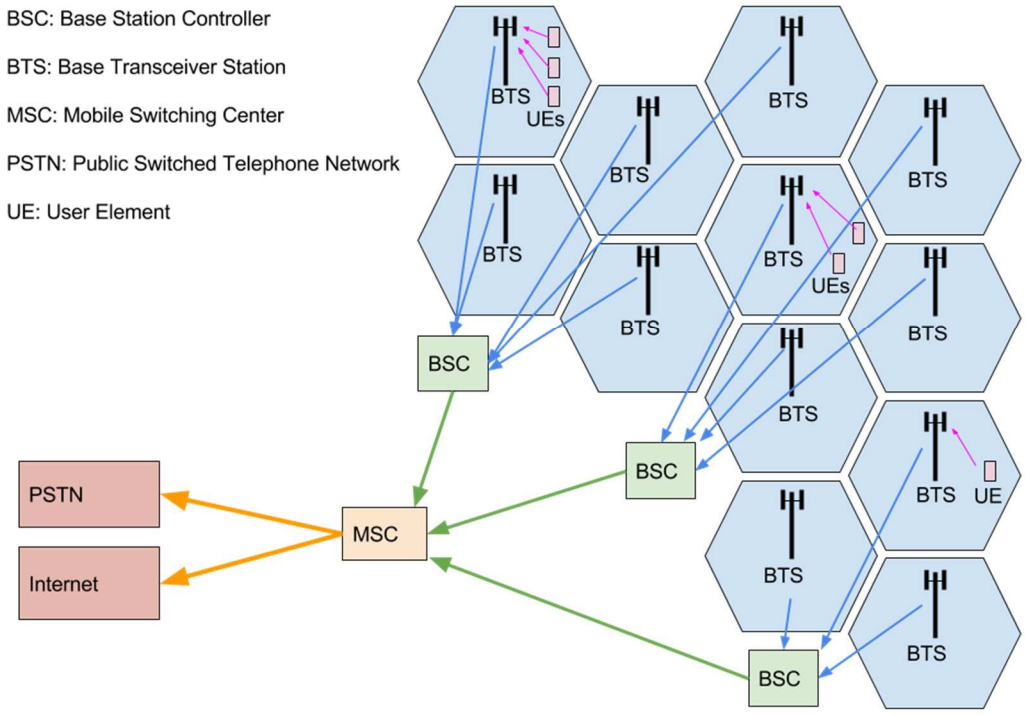

Figure 1. Diagram of a cellular network showing the division of the network into cells, each governed by its own base station as adapted from [7]

1.2. 5G and the Future of Wireless Communications

The future generations of wireless communications will need to incorporate even more users requesting access to more and more data. Furthermore, with the rise of the Internet of things and remote sensor networks, machine-to-machine traffic is expected to rise. Because of this required increase in capacity and the current number of competing technologies, the fifth generation of mobile service (5G) is expected to provide a platform that will allow for a "fully mobile and connected society" [7].

Radio	Network	Operations & Management
Leverage Spectrum • Exploit unlicensed spectrum and millimeter wave technology • C/U-path split, UL/DL split, multiple connectivity Enable cost-effective dense deployments • Integrate third-party deployments • Automate configuration, optimization, and healing • Multi-RAT coordination Coordinate and cancel interference • Massive MIMO • Exploit controlled non-orthogonal interfaces Support dynamic radio topology • Moving cells, relays, hubs, C-RAN, D-RAN • D2D Support	Create common composable core • Minimize number of entities and functionalities • Lean protocol stack • No mandatory U-plane functions • Minimize legacy interworking • RAT-agnostic core • Fixed and mobile convergence	Simplify operations and management • Automation and self-healing • Probeless monitoring • Collaborative Management • OAM functionality • Carrier-grade network control orchestration
Flexible functions and capabilities • Network slicing • Function variance • Flexible functions • Leverage NFV/SDN • State-disintegrated functions • Graceful degradation Support new value creation • Big data and context awareness • Expose radio and network APIs • XaaS (anything as a service) Build in security and privacy • C-plane security (e.g. HetNets) • Ensure location privacy and identity protection from unlawful disclosure		

Figure 2. Areas for improvement in 5G versus its predecessor technologies as adapted from [8]

Figure 2 highlights the three main areas that 5G will likely leverage to improve network capacity and end user experience [8]. The overarching theme is that 5G must

embrace flexibility at all levels of network design. This will allow it to operate in dense urban areas as well as rural ones and provide a diverse user base with high speed access to mobile data. Security is another critical feature that must be considered with the fifth generation mobile network and must be considered at all levels of system design from network architecture to physical layer radio link connections [8].

From the operations and management standpoint, 5G must make several key improvements over previous generations of cellular networks. Firstly, the network must be self-healing [8], which means it can respond to equipment failure in one area of the network or an intense strain in certain areas by balancing the load among the appropriate resources. Probeless monitoring is another important feature [8], which means that to diagnose and analyze network problems dedicated hardware will not be required; instead, network nodes can send data via a higher network layer to an endpoint that provides analysis for the entire network. Furthermore, collaborative management is required to ensure that the network can be operated across corporate and international boundaries and that the needs of all users are served [8].

From the network perspective, the goal is to create a simple and streamlined network core to increase network speeds. This can be achieved by reducing the number of entities and their functionalities and creating a lean protocol stack to decrease processing overhead [8]. Furthermore, legacy support can be minimized to reduce the need to slow down to support older hardware and older protocols. Most importantly the network core should not depend on the radio access technology used at the network's periphery, which

may vary depending on the current needs of a particular location. Furthermore, the idea that there should be no differentiation in service between wireline and wireless connections is central to 5G [8].

The radio technology used in 5G will also need to transform to support the large number of users and the bandwidth they demand. This growth in network traffic will require new and innovative wireless transmission schemes to provide faster and more reliable wireless connection than ever before in human history. To provide quality of service a dynamic radio topology is required that will support moving calls and integrate third party networks of hubs, picocells, and femtocells. Moreover, new unlicensed spectrum is being explored with large amounts of previously untapped bandwidth [9]. This millimeter wave technology utilizes spectrum around 60GHz, and although fading and attenuation is a large problem, the capacity gains across a good channel could be enormous. Furthermore, the transmission technology used must be scalable and able to adapt to changing link conditions [10]. In order to provide high data rates regardless of the spectrum or wireless topography being used, it is also likely that non-orthogonal communication systems will be deployed in 5G [11] [12] [13] [14]. Non-orthogonal systems introduce self-interference in order to increase system capacity. Although many proposed schemes like NOMA are new to the field of wireless networking, others such as MIMO have been used wirelessly for years. This thesis will focus on two non-orthogonal schemes: MIMO and FTN, and the potential capacity increases of a combined system.

1.3. MIMO and FTN Systems

To meet the stringent capacity requirements put forth for 5G, it is likely that non-orthogonal transmission schemes will be used [11] [12] [13] [14]. In an orthogonal transmission system, each transmitted symbol has its own allocated time or frequency and there is no inter-symbol interference. However, in a non-orthogonal communication system, inter-symbol interference is purposely induced to send more symbols in a given resource [15]. This increased number of transmitted symbols leaves the potential for capacity gains when compared with traditional signaling schemes. This thesis will look at two non-orthogonal transmission technologies: FTN and MIMO.

FTN systems have recently been explored in [14] [15] [16] [17] [18]. FTN systems can increase capacity by allowing transmitted symbols to overlap in the frequency or time domain. Figure 3 shows an example of symbol timings in a time domain FTN system and an orthogonal communication system. It can be observed that more symbols can be transmitted in a given amount of time which indicates a potential increase in capacity. The down side to this FTN is that the interference between transmitted symbols is increased because now each symbol overlaps with another in the time or frequency domains. This interference can be mitigated by error correction coding and clever receiver design, but it puts an upper bound on the capacity gains that can be achieved by such a system. Another consideration for FTN systems is receiver complexity, which increases linearly with the number of transmitted FTN streams. FTN systems can also compress pulses in the frequency domain as shown by Rannie [19], but this thesis will only focus on time-domain

FTN. A current example of a real world FTN system is Huawei's 400G long haul sub-sea field trial, which utilized FTN in an optical communication system [20].

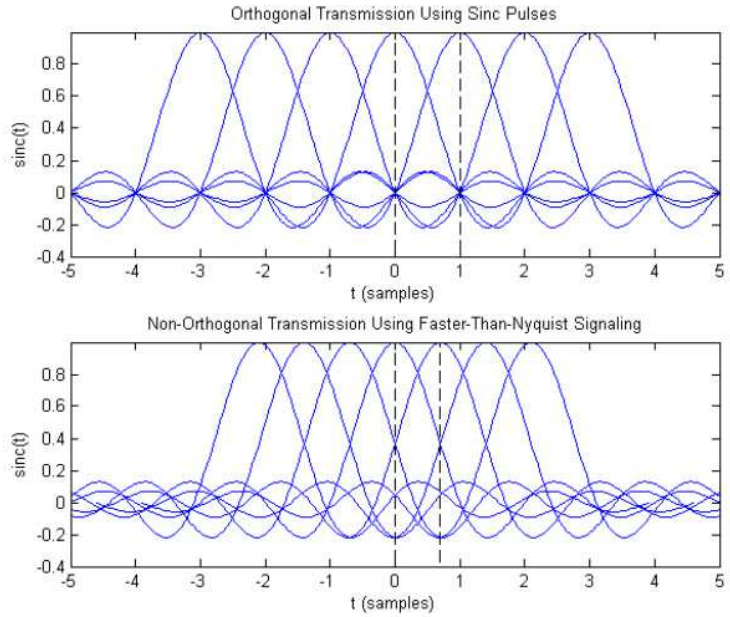

Figure 3. Example of transmitted pulses in Nyquist rate and time-domain FTN systems

MIMO is used to describe a channel with one or more inputs and one or more outputs. A classic example in wireless communications is a system with multiple transmitting antennas and multiple receiving antennas. Figure 4 shows a graphical representation of a system with three transmitting antennas and three receiving antennas. It shows how a copy of the signal from each transmit antennas is received at each receiving antenna. This means that interference between the signals received from each antenna exists at the receiver. If nothing about the channel is known, the same data can be transmitted on all transmitting antennas to increase the number of paths over which the

signal will propagate to reach the receiver. Even if one of the paths is suffering from fading, the likelihood that good path to the receiver exists is increased. Furthermore, the receiving antennas would provide diversity reception by receiving the signal at spatially diverse locations; once again decreasing the probability that a signal will get lost due to a fade [21]. This scheme, however, does not constitute non-orthogonal transmission since the same signal is being transmitted on all antennas. If knowledge of the channel gains between each transmitting and receiving antenna is known, different signals can be transmitted simultaneously at each antenna and the receiver can use its channel knowledge to decode the received signals [21] [22]. Even though there is now interference between transmitted signals, the capacity is increased because multiple symbols are being transmitted simultaneously. Furthermore, if the transmitter has knowledge of the channel, it can pre-code its transmitted signal to provide a further increase in capacity [21].

There is a tradeoff in performance associated with choosing between a MIMO system with diversity reception, and a MIMO system that uses non-orthogonal transmission to increase its number of degrees of freedom and thereby its capacity [23]. By designing a system to take full advantage of spatial diversity, a low bit error rate can be achieved, but the channel capacity is not improved. Likewise, using increasing the number of degrees of freedom across a MIMO channel does not improve the system's bit error rate. According to Tse [23], a system with a sufficient number of antennas can be designed to perform both diversity reception using some antennas and increase its number of degrees of freedom using other antennas; this allows for a compromise between the strengths of these two techniques when designing a MIMO system [23].

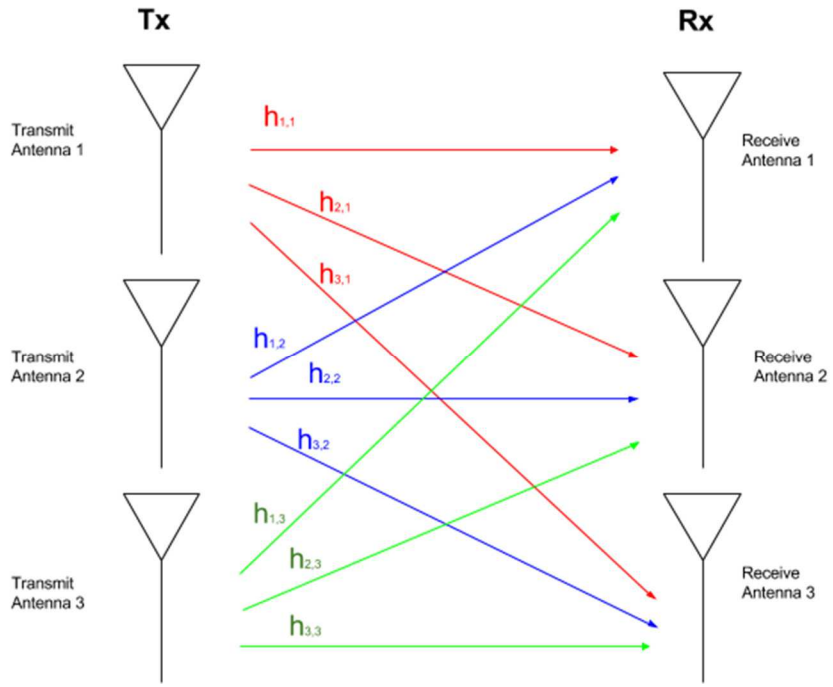

Figure 4. Graphical representation of a MIMO system with three transmitting antennas and three receiving antennas; $h_{i,j}$ corresponds to the channel gain between the *i*th receive antenna and the *j*th transmit antenna

1.4. Thesis Contributions

MIMO and FTN systems have been researched independently of one another for years. Both systems demonstrate capacity gains when compared to their orthogonal counterparts. This thesis seeks to combine MIMO and FTN techniques to create a system with even larger capacity gains. This has been demonstrated before by Rusek by analyzing the Mazo limit for such systems [24] [25]. However, this thesis will follow up on research into transmitting multiple FTN streams simultaneously with the addition of MIMO [1].

Furthermore, alternative receiver architectures are explored and their capacity compared with that of an orthogonal communication system. A brief overview of the sections of this thesis is presented in the following paragraphs

Chapter 2 is a review of previous research into MIMO and FTN systems. It introduces the system architecture for both MIMO and FTN systems independently. Furthermore, it introduces the methods for calculating the Shannon capacities of such systems. For MIMO, systems with channel state information at the receiver and channel state information at the transmitter are considered.

Chapter 3 introduces combined FTN MIMO systems when channel state information is only known to the receiver and known to both the transmitter and the receiver. A simple combined architecture is introduced and the Shannon capacity of the system is derived. Results relating the capacity of the combined FTN MIMO system, a MIMO only system, and an FTN only system are provided. Furthermore, an 'orthogonalized' receiver architecture is proposed for the system. This architecture relies on a higher sampling rate at the receiver to reduce the complexity of the receiver. The capacity of this architecture is derived and the results are compared with those of existing systems. An 'undersampled' architecture is also put forth that attempts to use a minimalistic receiver for recovery of an FTN MIMO signal. The capacity of this architecture is also derived and the capacity results are compared with those of the former two systems.

Chapter 4 provides a summary of the research conducted in this thesis and puts forward several possible avenues for future research.

Chapter 2. Prior Work

This chapter presents an overview of FTN and MIMO system architectures that currently appear in literature. The goal is to give the reader a fundamental understanding of these systems and their capacity limits.

2.1. Introduction to MIMO Architectures

Out of the many techniques to increase the capacity of a communication system, MIMO has received particular interest over the last decade. MIMO does not require additional bandwidth nor additional transmitter power. Rather, it makes use of multiple spatial streams to increase the capacity of a system.

2.1.1 MIMO System Block Diagram

Figure 5 shows the basic MIMO architecture with n_T transmitting antennas and n_R receiving antennas. In this MIMO system, n_T bits are transmitted simultaneously. These bits are represented by $x_{i,n}$ where n refers to the nth bit in the sequence of transmitted bits on the ith transmitting antenna. Each bit is modulated by a pulse $p(t)$. This pulse shaping is similar to what would occur in a SISO system; a sinc pulse will yield maximum bandwidth efficiency but is physically impossible to implement because it is non-causal. In reality a root-raised cosine pulse (as found in GSM) or a rectangular pulse (as found in Wi-Fi) would likely be used. Thus, the transmitted signal at antenna i can be expressed in (1) for transmitted packet length of N.

$$x_i(t) = \sum_{n=0}^{N} x_{i,n}\, p(t - nT) \tag{1}$$

As the transmitted signal propagates it experiences attenuation and phase shift. In multipath scenarios, multiple copies of the same signal will arrive at each receiving antenna. Assuming the coherence time is less than the symbol time *T*, it is possible to write the incoming signal from a single source at each antenna as the original transmitted signal multiplied by some complex attenuation factor $h_{i,j}$ where *i* is the index of the transmitting antenna and *j* is the index of the receiving antenna. Because an individual receiving antenna receives signals from all n_T transmit antennas attenuated by some factor, it is necessary to express the received signal at each antenna as a sum of the signal received from each individual signal source. In addition, the receiver's analog amplifier circuitry causes AWGN noise $\nu(t)$ to be added to the received signal. Thus, the received signal $r_j(t)$ on each antenna *j*, can be expressed in (2).

$$r_j(t) = \sum_{i=1}^{n_T} h_{i,j}\, x_i(t) + \nu(t) \tag{2}$$

The received continuous time domain signal is then passed through a filter matched to the complex conjugate of the modulating pulse to maximize the signal to noise ratio when received signal at the output of the matched filter is sampled. The received signal at the filter output on the *j*th antenna is represented by $y_j(t)$ and can be expressed by (3). Due to the properties of AWGN, this matched filtering does not lead to any amplification of the noise power if the noise is uncorrelated and no inter-symbol interference is present.

$$y_j(t) = p^*(-t) * (r_j(t) + \nu(t))$$
$$y_j(t) = \sum_{i=1}^{n_T} \sum_{n=0}^{N} p^*(-t) * h_{i,j} x_{i,n} p(t - nT) + \nu(t) \quad (3)$$

In these equations, the * operator represents convolution.. After matched filtering, the continuous time signal is sampled to become a discrete signal. In this MIMO architecture, the signal is sampled at time *mT* where *m* ranges from 0 to packet length *N*. Notice that by sampling at this interval, the discrete time output of the sample and hold device can be expressed by equation (4).

$$y_j[m] = \sum_{i=1}^{n_T} \sum_{n=0}^{N} p^*(-t) * h_{i,j} x_{i,n} p(t - nT) + \nu(t) |_{t=mT} \quad (4)$$

$$\int_{-\infty}^{\infty} p^2(t) = 1 \quad (5)$$

$$y_j[m] = \sum_{i=1}^{n_T} \sum_{n=1}^{N} h_{i,j} x_{i,n} |_{t=mT} + \nu[m] \quad (6)$$

If the modulating pulse is selected to be a unit energy pulse such that equation (5) holds true, then the expression in (4) can be simplified to (6), since value of the convolution between the modulating pulse and it's matched filter will evaluate to 1 at the sample times *mT*.

Because there is no inter-symbol interference, the sum over all transmitted pulses in the packet evaluated at times *mT* only depends on the instance where *n* is equal to *m.* This means that sum can be eliminated and equation (6) now takes its final form as (7).

$$y_j[n] = \sum_{i=1}^{n_T} h_{i,j} x_{i,n} + \nu[n] \quad (7)$$

In a traditional SISO communication system, a threshold device can be used to map each *y[n]* to the appropriate bit(s). However, in this MIMO communication system, because the received signal on one antenna contains a copy of the transmitted signal from each transmit antenna, a simple threshold device can no longer be used. The output from each receive antenna signal chain must be combined and a soft decision must be made.

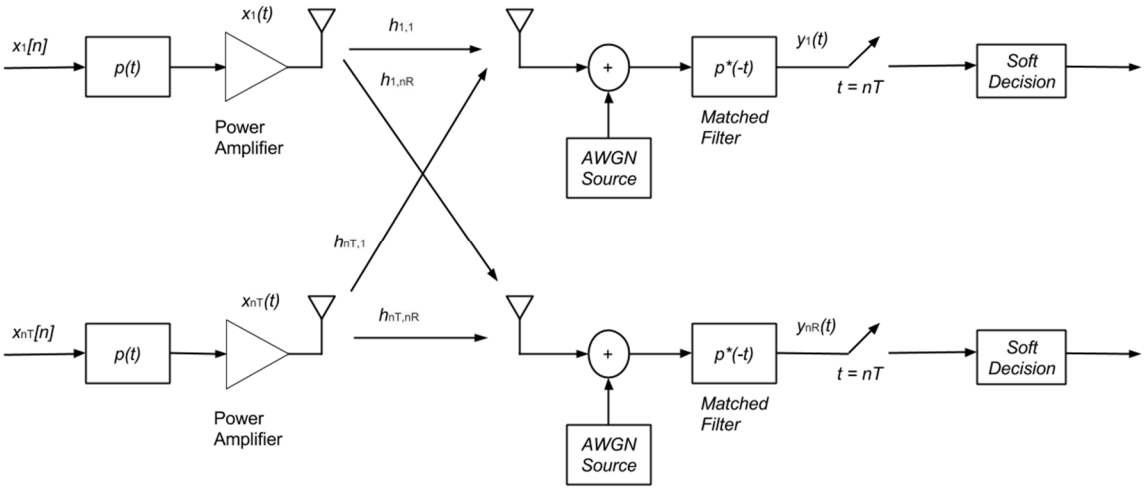

Figure 5. Block diagram of A MIMO communication system with n_T transmitting antennas and n_R receiving antennas

Assuming the receiver has knowledge of the path $h_{i,j}$ between the *i*th transmit antenna and the *j*th receive antenna, a channel matrix **H** can be described as (8).

$$\mathbf{H} = \begin{pmatrix} h_{1,1} & \cdots & h_{1,n_T} \\ \vdots & \ddots & \vdots \\ h_{n_R,1} & \cdots & h_{n_R,n_T} \end{pmatrix} \tag{8}$$

The receiver can obtain this knowledge if the transmitter sends a predifined test sequence before beginning data transmission. The receiver can analyze the received test sequence and determine each of the channel coefficients. In this case it is assumed that the coherence time of the channel is much longer than the period of a single bit, thus entire packets can be transmitted and decoded using one set of channel measurements. As more reflectors and refractors in the environment move at greater speeds, this asumption becomes invalid

From this we can vectorize the expression for the received signal. The transmit vector **x**, the receive vector **y**, and the noise vector **n**, are defined in (9). These vectors correspond the channel inputs and outputs at a single time *n*.

$$\mathbf{x} = \begin{pmatrix} x_1 \\ \vdots \\ x_{n_T} \end{pmatrix}, \mathbf{y} = \begin{pmatrix} y_1 \\ \vdots \\ y_{n_R} \end{pmatrix}, \mathbf{v} = \begin{pmatrix} v_1 \\ \vdots \\ v_{n_R} \end{pmatrix} \tag{9}$$

In (7) we showed that because we are describing a case without inter-symbol interference, each received $y_j[n]$ only corresponds to the transmitted signal x for one value of n. As a result, the input to output relationship can be analyzed at one time n and the expression in (7) can now be rewritten as (10).

$$\mathbf{y} = \mathbf{H}\mathbf{x} + \mathbf{n} \tag{10}$$

The transmit, receive, and noise vectors each have their own covariance matrix, which describes the covariance between each of the entries in the vectors. The structure of these covariance matrices will be important when calculating the channel capacity.

2.1.2 Considerations for Antenna Design and Arrangement

Ideally the entries in the channel matrix **H** should be independent because this means that the system can take advantages of instances where one path is subjected to a high degree of fading, but the other paths still have negligible attenuation. To achieve this, each antenna must be at least a half wavelength away from its neighbors to ensure different scattering and multipath properties for the signal it transmits and receives [21].

In practice there are several models used to generate the **H** matrix, each depending on different real-world scenarios. In this paper the entries in **H** are assumed to be real independent identically distributed Gaussian variables with a mean of zero and variance of one [21]. This is also referred to as the ZMSW (Zero Mean Spatially White) model. According to [26], the advantage of this model is that it can show the long term average of channel distribution coefficients in many different environments.

Other models for **H** include Jake's model, which takes the radiation pattern of each antenna and the structure of the array into account [27].

2.2. Ergodic Capacity of MIMO Systems

Using the MIMO system described in Section 2.1, an upper bound for the system's ergodic capacity can be calculated. We will find the system capacity in two different scenarios: channel state known only at receiver (CSIR) and channel state known at both transmitter and receiver (CSIT).

2.2.1 Capacity of a MIMO System with CSIR

To calculate the Shannon capacity of a CSIR MIMO system, it is necessary to start with (11) [28]. The channel capacity C is defined as the maximum mutual information from the transmitted message **X** and the received message **Y** over all possible realizations of the transmitted message **X**. In turn, the mutual information between **X** and **Y** is defined as the difference between the entropies of **Y** and **Y** given **X**. In equation (11), $p(\mathbf{X})$ is used to indicate that this is the maximum mutual information from input to output across all possible input distributions.

$$C = \max_{p(\mathbf{X})} I(\mathbf{X};\mathbf{Y}) = \max_{p(\mathbf{X})}[H(\mathbf{Y}) - H(\mathbf{Y} \mid \mathbf{X})] \tag{11}$$

The entropy of the channel output **Y** is defined in (12) and the entropy of the conditional output **Y** given **X** is defined in (13). In these equations, **Y** represents the vector of received signals from $y_1 \ldots y_{nR}$ and **y** represents a single value in this vector; **X** represents vector of transmitted signals $x_1 \ldots x_{nT}$ and **x** represents a single value in this vector. The probabilities $p(\mathbf{y})$ and $p(\mathbf{x},\mathbf{y})$ are the probabilities of a particular instance of **y** or both **y** and **x** occurring respectively. These entropies are defined across an entire vector instead of a single random variable as in SISO capacity. For the AWGN channel considered in this thesis, $H(\mathbf{Y}|\mathbf{X})$ must be equal to the entropy in the noise $H(\mathbf{n})$ by the definition of entropy.

$$H(\mathbf{Y}) = -\sum_{\mathbf{y}\in\mathbf{Y}} p(\mathbf{y}) \log_2(p(\mathbf{y})) \tag{12}$$

$$H(\mathbf{Y} \mid \mathbf{X}) = -\sum_{\mathbf{x}\in\mathbf{X},\mathbf{y}\in\mathbf{Y}} p(\mathbf{x},\mathbf{y}) \log_2(p(\mathbf{y} \mid \mathbf{x})) \tag{13}$$

The covariance matrix of the received signal vector $\mathbf{Q_y}$ can be written as $\mathbf{E}[\mathbf{yy}^H]$ because the $\mathbf{y}$ has zero mean. If the covariance matrix of the of the transmitted signal vector $\mathbf{Q_x}$ is known, the $\mathbf{Q_y}$ can be expressed in equation (14) where $\mathbf{H}$ is the channel matrix for the MIMO system.

$$\mathbf{Q}_\mathbf{y} = \mathbf{H}\mathbf{Q}_\mathbf{x}\mathbf{H}^H + \mathbf{I}_{n_R} \tag{14}$$

In equation (14) the unscaled identity matrix is used because we are assuming that the noise variance is one. The power in the noise will be taken into account later in the covariance matrix $\mathbf{Q_x}$. The identity matrix is a diagonal matrix of size n_R by n_R whose non-zero entries are all one.

If the received vector $\mathbf{y}$ is composed of zero-mean, circularly symmetric complex Gaussian entries, then the entropy of the received signal vector is maximized. The only way for $\mathbf{y}$ to be a zero-mean, circularly symmetric complex Gaussian vector is if the transmitted vector $\mathbf{x}$ is also zero-mean, circularly symmetric complex Gaussian. This means that the entropy of $\mathbf{Y}$ can be written in (15) while the entropy of the noise is simply expressed in (16). In these equations, B represents the channel bandwidth.

$$H(\mathbf{Y}) = B\log_2(\det[\pi e\mathbf{Q}_y]) \tag{15}$$

$$H(\mathbf{n}) = B\log_2(\det[\pi e\mathbf{I}_{n_R}]) \tag{16}$$

Thus the mutual information between the transmitter and receiver can be expressed as (17).

$$I(\mathbf{X};\mathbf{Y}) = B\log_2(\det[\mathbf{I}_{n_R} + \mathbf{H}\mathbf{Q}_x\mathbf{H}^H]) \tag{17}$$

If the system is operating with the channel state known only to the receiver, then the transmitter does not know the optimal way to allocate power among the transmit antennas. In this case, the best the transmitter can do is to allocate power equally among all transmit antennas. The covariance matrix of the transmit vector, $\mathbf{Q_x}$, can be expressed as (18).

$$\mathbf{Q}_x = \frac{P_T}{n_T \sigma^2} \mathbf{I}_{n_T} \tag{18}$$

In equation (18) P_T is the total transmit power and it is equally divided across n_T antennas. Another assumption is made that the AWGN noise power σ^2 is the same on all receiving antennas. Since there is likely some consistent use of hardware between all receive antennas, this is generally a valid assumption to make. This power allocation scales an identity matrix because the information transmitted at each antenna is independent of that transmitted at the others. Thus the symbols sent at one antenna are uncorrelated with those of their neighbors. With this expression for $\mathbf{Q_x}$ the mutual information between the transmitter and receiver can now be rewritten as (19).

$$I(\mathbf{x};\mathbf{y}) = B \log_2 (\det \left[\mathbf{I}_{n_T} + \frac{P_T}{n_T \sigma^2} \mathbf{H}\mathbf{H}^H \right]) \tag{19}$$

This can be substituted into the original expression for channel capacity to yield equation (20).

$$C = \sup \left(B \log_2 \left(\det \left[\mathbf{I}_{n_R} + \frac{P_T}{n_T \sigma^2} \mathbf{H}\mathbf{H}^H \right] \right) \right) \tag{20}$$

However, this is not the final form of the MIMO CSIR capacity equation. In this thesis, the normalized capacity is used with units of bits / sec / Hz. Thus, the bandwidth B can be dropped from the right hand side of (20). In addition, the expression in (20) only gives the capacity for one realization of a MIMO channel matrix. In reality, depending on the location of the transmitter and receiver and the distribution of reflectors in the environment, the MIMO channel matrix can have many possible realizations. Because of this, it is necessary to use ergodic capacity and take the expected value of the system capacity over all realizations of the MIMO channel matrix. Thus the final form of the MIMO CSIR capacity equation is expressed in (21).

$$C = E\left[\sup\left(\log_2\left(\det\left[\mathbf{I}_{n_R} + \frac{P_T}{n_T\sigma^2}\mathbf{H}\mathbf{H}^H\right]\right)\right)\right] \tag{21}$$

Figure 6 illustrates the capacity gains from MIMO systems with respect to the SISO case. In this figure, one thousand instances of the channel matrix **H** were generated using the ZMSW model defined earlier. The average channel capacity resulting from all thousand instances was then plotted at each SNR value. This figure shows that for increasing MIMO order, the system capacity is increased. It can also be observed that the increase is greater at higher SNRs than lower ones.

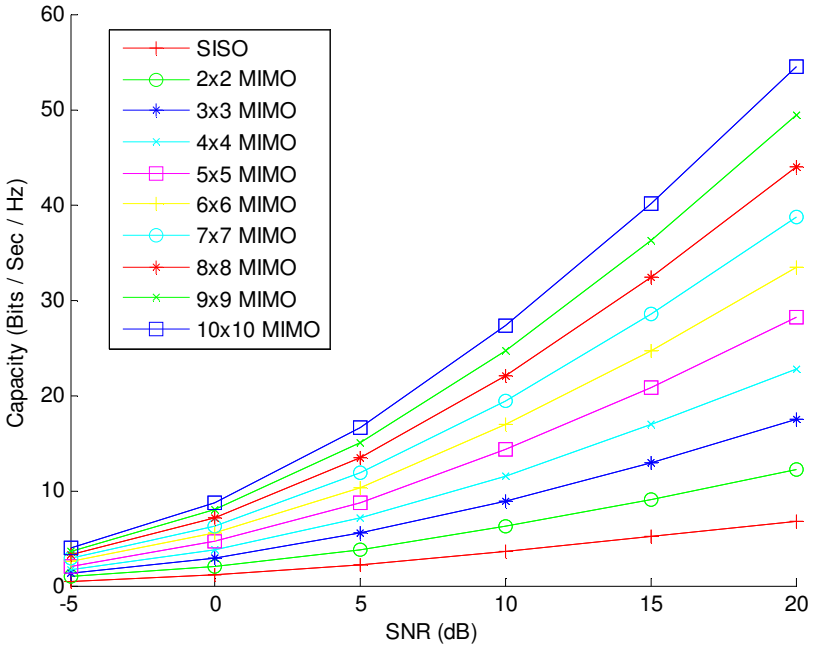

Figure 6. Capacity comparison of MIMO systems with n_T=n_R=1…10

A MIMO system can also be used when the number of transmitting antennas is greater than the number of receiving antennas. Figure 7 demonstrates this by showing the capacities for systems with multiple transmit antennas and only one receiving antenna. It can be observed that there is no significant capacity gain by increasing the number of transmitting antennas without also increasing the number of receiving antennas. An intuitive method of understanding this is that more transmitting antennas may allow the transmitter to send more data simultaneously, but if the number of receiving antennas does not increase, the interference between transmitters has increased without providing any additional information at the receiver.

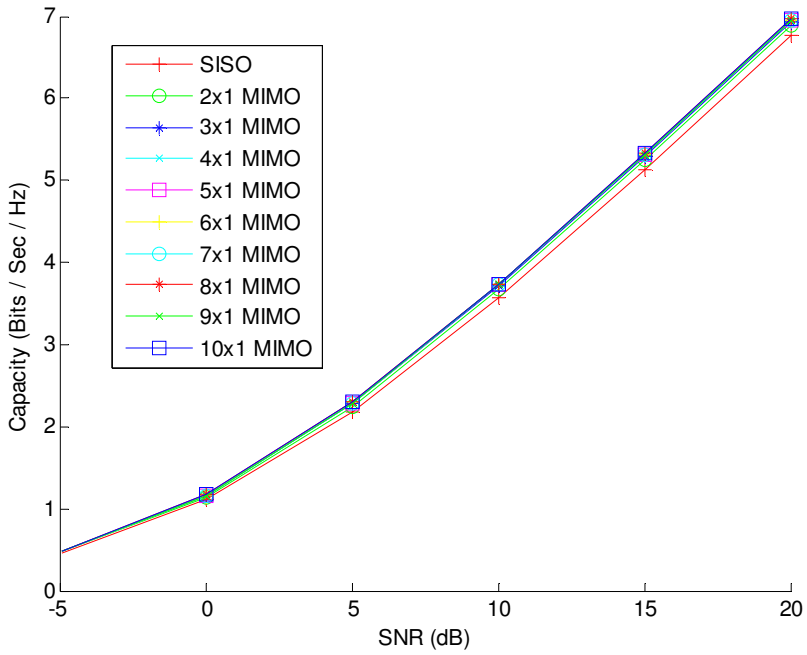

Figure 7. Capacity comparison of MISO systems for n_T=1…10

MIMO systems can also have more receiving antennas than transmitting antennas. Figure 8 shows capacities for systems with only one transmitting antenna and multiple receive antennas. It can be observed that there is a somewhat significant capacity increase by adding receive antennas, but the effects are not as pronounced at high SNRs; the benefits of extra receive antennas suffers from diminishing returns.

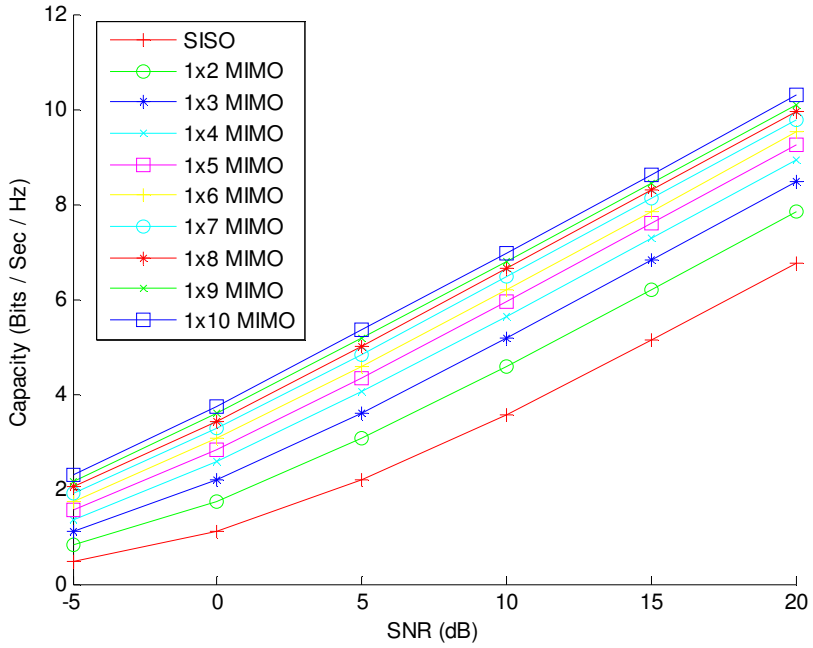

Figure 8. Capacity comparison of SIMO systems for n_R=1…10

To demonstrate the differences in capacity gains for different MIMO configurations, Figure 9 plots the capacity of SISO, 1x2 MIMO, 2x1 MIMO, and 2x2 MIMO systems. From this plot it can be observed that the 2x2 MIMO system yields the greatest capacity, especially at high SNRs. The 1x2 MIMO system performs comparably at low SNRs but does not have the same capacity increase as the 2x2 MIMO system for higher SNRs. The 2x1 MIMO system has a slight gain compared to the SISO case, but is not comparable to the other MIMO systems.

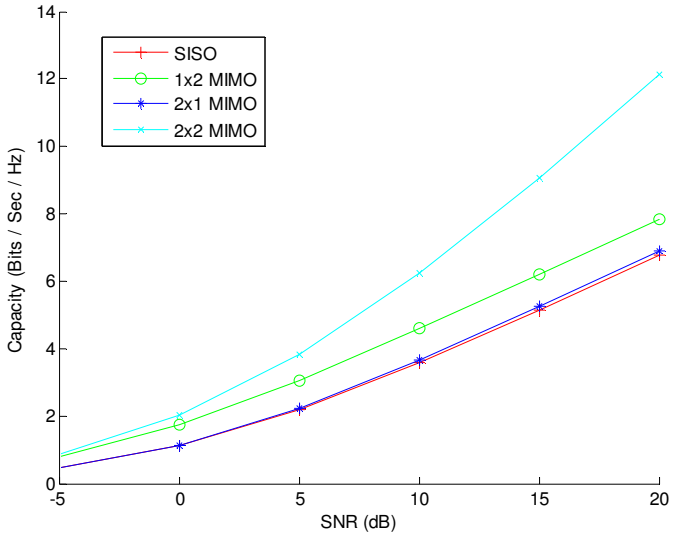

Figure 9. Capacity comparison of a SISO system, 1x2 SIMO, 2x1 MISO, and a 2x2 MIMO system

2.2.2 Capacity of a MIMO System with CSIT

Capacity gains compared to SISO can be observed with channel state information known only at the receiver. However, if the transmitter also had channel knowledge, it could precode the transmitted signal to achieve optimum capacity. In this section an expression for the capacity of MIMO with CSIT is derived and compared with the CSIR result in the previous section.

Equation (19) was derived for the mutual information of a MIMO channel with a given channel matrix **H**. If channel knowledge, that is, the channel matrix, is known at the transmitter, then the transmitter can perform a singular value decomposition on the channel matrix to determine the number and the quality of parallel Gaussian channels. The singular values of the channel correspond to parallel Gaussian channels between the transmitter and the receiver. Singular values with a greater magnitude represent a channel with a greater

gain. Once the transmitter has this knowledge, it can determine the optimal power allocation for each of the parallel Gaussian channels. For example, the mutual information given in (19) can be written as (22) where σ_i^2 is the *i*th singular value of the channel matrix **H**, P_i is the power allocated to an individual channel, and n is the number of parallel Gaussian channels resulting from the decomposition of matrix **H**.

$$I(\mathbf{X};\mathbf{Y}) = \sum_{i=1}^{n} B\log_2(1+\sigma_i^2\frac{P_i}{\sigma^2}) \tag{22}$$

The number of singular values of an instance of the channel matrix corresponds directly to its rank, thus a full rank matrix should optimize channel capacity. When the channel matrix is full rank, the system is said to be in a 'rich scattering environment' [21]. A matrix's rank cannot exceed the minimum number of columns and number of rows, so the number of parallel Gaussian channels can be increased by increasing the lesser of the number of transmitting or receiving antennas.

In the case with no channel state information known at the transmitter, the best allocation scheme the transmitter can use is to allocate power equally across all the Gaussian channels. However, if channel state information is known at the transmitter, the water-filling algorithm can be used to allocate power among the parallel channels such that the system capacity is maximized. The water filling algorithm allocates more power to channels with high SNRs and less power (or no power at all) to channels with lower SNRs. Figure 10 helps to visualize this process. After the channel decomposition, the singular values represent the SNRs of their respective Gaussian channels. The singular values can

then be inverted and plotted on a set of axes. To determine the power allocation among these channels, the plot can be imagined as a bowl or a lake. All the power available to the transmitter is like water which is poured into the lake and at settles at a certain level. After the water settles, the deepest portions of the lake will have the most water above them and the lowest portions of the lake will have the least. This corresponds to the best channels receiving proportionally more power than the worst channels. In Figure 10, the red line indicates the water level after the water has settled. Note that some really bad channels will not receive any power allocation whatsoever. The water filling algorithm must be re-run for each realization of the MIMO channel matrix.

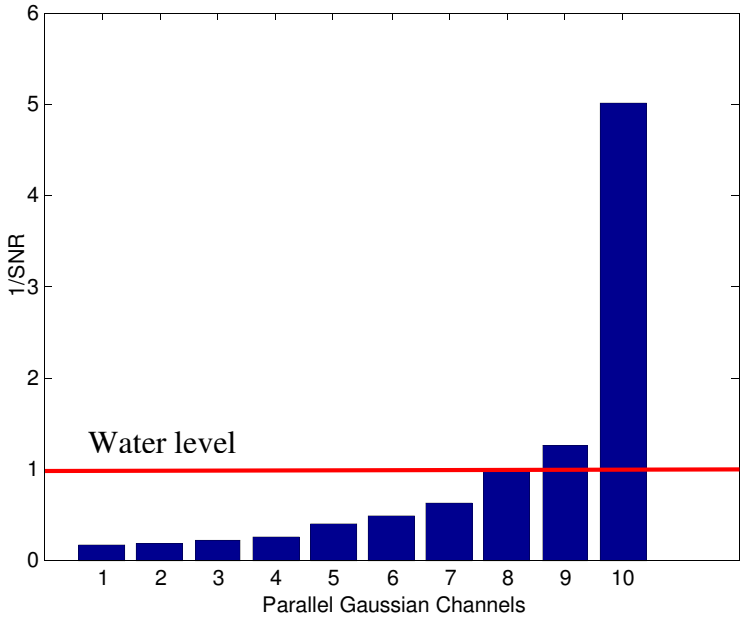

Figure 10. Graphical representation of the water filling algorithm: the height of each parallel Gaussian channel corresponds to the inverse of its SNR and the water level corresponds to the power allocated to each channel

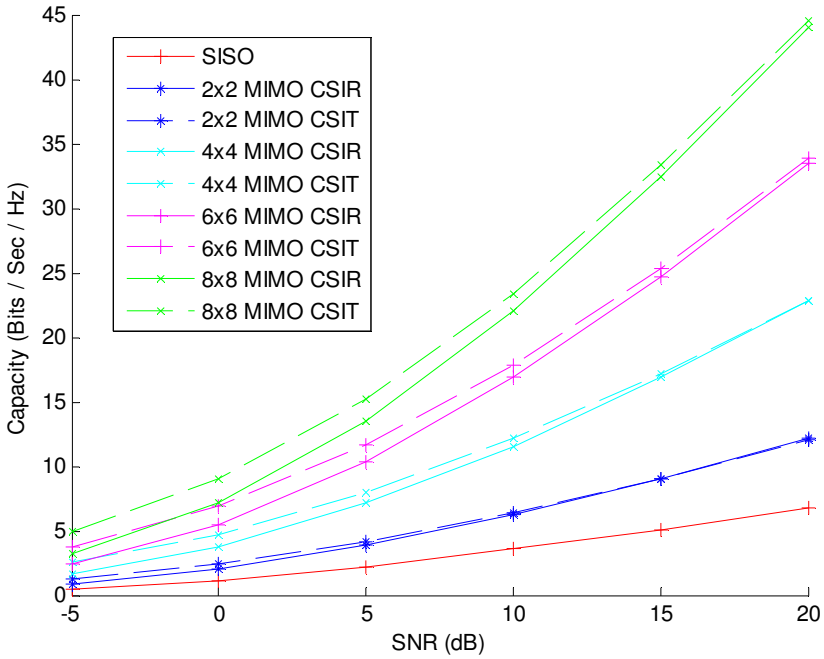

Figure 11. Comparison of MIMO systems with the same number of transmitters and receivers for CSIR and CSIT

Figure 11 compares the capacity of MIMO systems with CSIR and CSIT for varying number of antennas. In this figure it can be observed with CSIT as with CSIR, the channel capacity greatly increases at high SNRs as the number of antennas increases. However, for 2x2MIMO systems with the same number of antennas, CSIT does little to improve the capacity at high SNRs compared with the CSIR version of the same system. CSIT's strength is that at low SNRs, it enables a significant capacity gain when compared with a CSIR systems with the same number of antennas. Moreover, as the number of antennas in the system increases, the gains at low SNRs between the CSIT system and the comparable CSIR system increase.

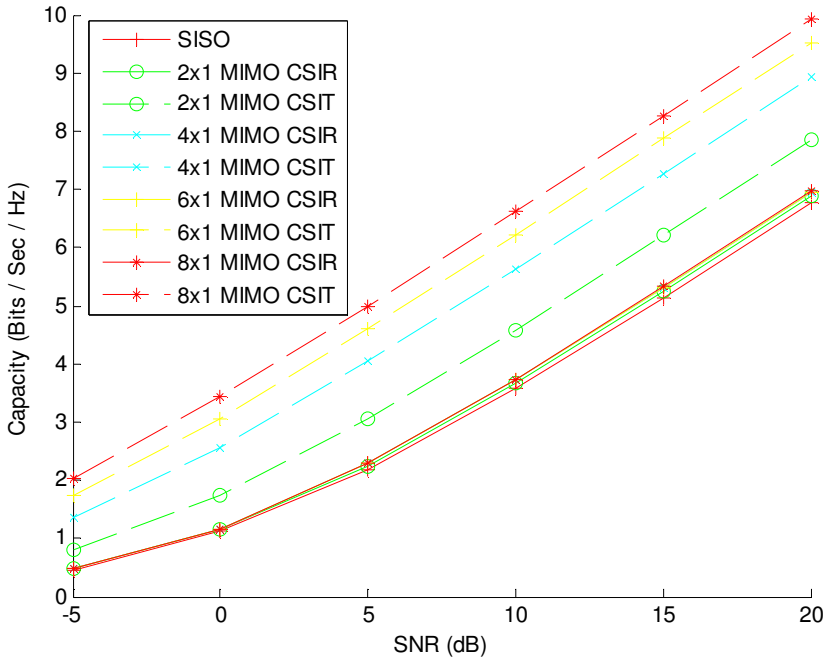

Figure 12. Comparison of MIMO systems with the more transmitting antennas than receiving antennas for CSIR and CSIT

Figure 12 compares MIMO systems with CSIT and CSIR where the number of transmitting antennas is greater than the number of receiving antennas. It can be observed for MIMO systems where the number of transmitting antennas is greater than the number of receiving antennas, the CSIT version of the system has the potential to significantly outperform the CSIR version of the system in terms of capacity. With CSIR little can be done to take advantage of the parallel Gaussian channels if there is only one receive antenna. However, with CSIT, the transmitter can allocate power optimally among the parallel channels while transmitting, allowing the system to take full advantage of this particular antenna configuration.

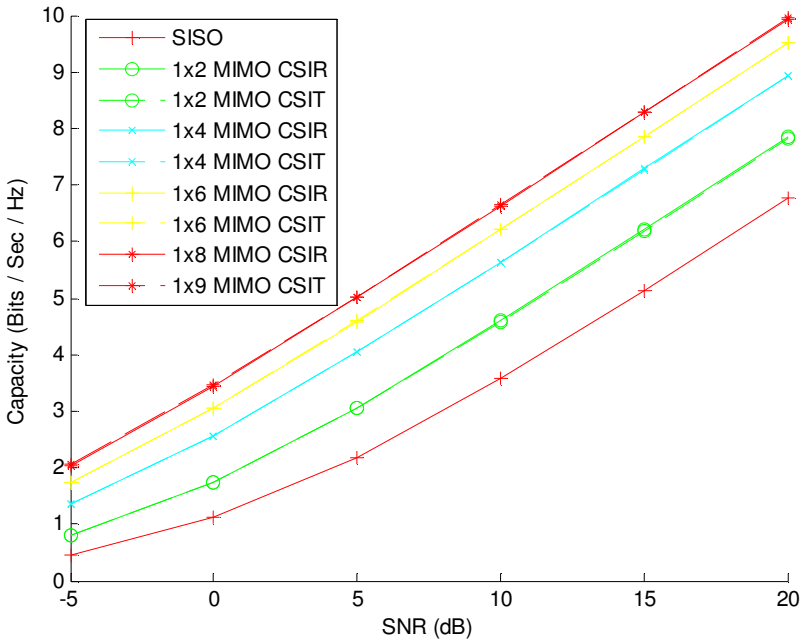

Figure 13. Comparison of MIMO Systems with more receiving antennas than transmitting antennas for CSIR and CSIT

Figure 13 compares the CSIT and CSIR capacities of MIMO systems with a larger number of receiving antennas than transmitting antennas. It can be observed that for two systems with the same antenna arrangement there is no significant capacity improvement between the CSIT and CSIR cases. In the case where there is only one transmit antenna, all power is simply allocated to that antenna and the MIMO capacity gains depend on the receiver's ability to perform diversity reception. In general, for systems with fewer transmit antennas, the transmitter's ability to perform power allocation is not as important as the detection performed at the receiver.

Figure 14 compares various MIMO systems with CSIR and CSIT to demonstrate the gains achieved if water filling is performed at the transmitter. It can be observed that for CSIT just as for CSIR, the largest capacity gains occur when the number of transmit and receive antennas are equal. However, with CSIT, the capacities when the system has more transmitting antennas or more receiving antennas are comparable. This means that in particular, asymmetric MIMO systems operating at low SNRs could see significant capacity improvements if channel state information is available at the transmitter and water filling is used to optimally allocate power among the parallel Gaussian channels.

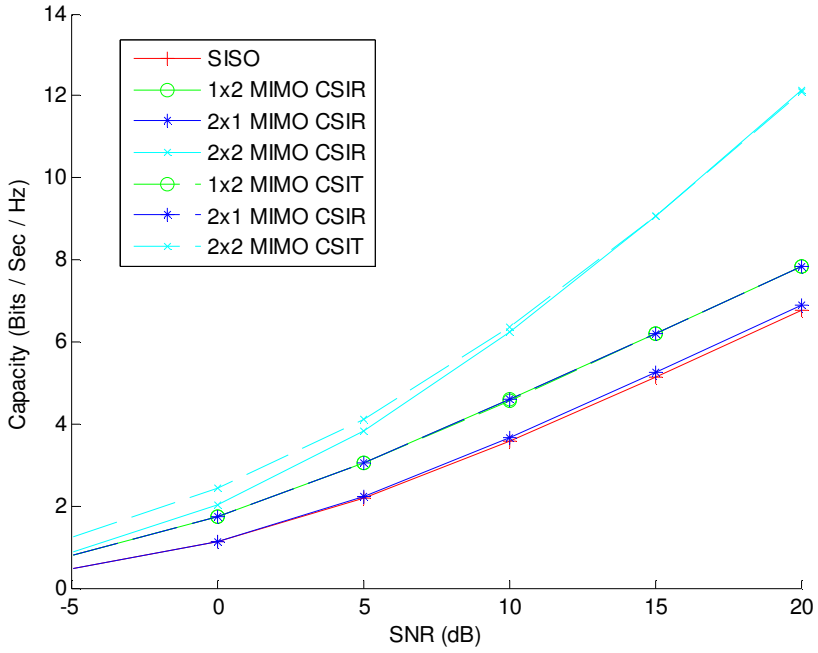

Figure 14. Comparison of a SISO system, 1x2 MIMO with CSIR, 2x1 MIMO with CSIR, 2x2 MIMO with CSIR, 1x2 MIMO with CSIT, 2x1 MIMO with CSIT, and 2x2 MIMO with CSIT

2.3. Introduction to FTN Architectures

Another type of non-orthogonal communication system is FTN .The Nyquist Limit says that for a given bandwidth, only a certain number of symbols per second can be recovered. In an orthogonal communication system, one symbol occupies its own time, frequency, or code slice. In a faster-than-Nyquist communication system multiple symbols can occupy the same time or frequency slice. In other words, ISI is intentionally introduced in the transmitted signal in an attempt to increase capacity. In this thesis, only time-domain FTN architectures will be analyzed as these were used in the conference paper [1] by Yuhas, Feng, and Bajcsy. In practice, frequency-domain FTN systems as described in [19] could be used in the same way, but that is a future area of research

2.3.1 Time-domain FTN System Architecture

Figure 15 shows the architecture of a basic time-domain FTN communication system. In this system k bit streams $x_{1,n}\ldots x_{k,n}$ are generated simultaneously at the transmitter. Thus the nth symbol on the ith stream is representd by $x_{i,n}$. Each transmitted bit is mapped to a symbol by modulating the waveform $p(t)$. Next, delayed copies of each bit stream are added together to form the transmitted waveform $x(t)$ expressed in (23). Note that the packet length for this system is Nk. Each stream is delayed by an amount less than one symbol time so that the streams are transmitted simultaneously. In this thesis, the case where the delays between consecutive bit streams are equal is analyzed. This means that the ith bit stream is delayed by $(i\text{-}1)T/k$ seconds, or that in Figure 15, tau is equal to $(i\text{-}1)T/k$.

$$x(t) = \sum_{n=1}^{N} \sum_{i=1}^{k} x_{i,n}\, p\left(t - (n-1)T - \frac{(i-1)T}{k} \right) \tag{23}$$

The waveform *x(t)* is transmitted across a channel. This system model uses an AWGN channel with no attenuation. The AWGN channel has an infinite bandwidth and an infinite coherence time so no power is lost in transmission across the channel. AWGN is added in the receiver amplifier circuits. The received signal can *r(t)* can be represented by (24) where *z(t)* is continuous time AWGN.

$$r(t) = \sum_{n=1}^{N} \sum_{i=1}^{k} x_{i,n} p\left(t - (n-1)T - \frac{(i-1)T}{k} \right) + z(t) \tag{24}$$

The received signal is then split into *k* copies for each bit stream. The *h*th copy is then delayed by (*h*-1)T/*k* seconds and matched filtered with a filter matched to *p(t)*. Just as in the MIMO system, the matched filter does not affect the amplitude of the AWGN as long as the noise is uncorrelated. The signal $y_h(t)$ at the output of the *h*th matched filter can be described by (25).

$$y_h(t) = e^{2\pi j \frac{h}{k}} \sum_{n=1}^{N} \sum_{i=1}^{k} x_{i,n} p\left(t - (n-1)T - \frac{(i-1)T}{k} \right) * p^*(-t) + z(t) \tag{25}$$

After each signal $y_h(t)$ is match filtered, it is sampled at *T* second intervals. The output $y_h[m]$ can be described by (26).

$$y_h[m] = e^{2\pi j \frac{h}{k}} \sum_{n=1}^{N} \sum_{i=1}^{k} x_{i,n} p\left(t - (n-1)T - \frac{(i-1)T}{k} \right) * p^*(-t) + z(t) \Big|_{t=mT+\frac{(h-1)T}{k}} \tag{26}$$

If the modulating pulse is unit energy, then at the sampling times the convolution of *p(t)* and its complex conjugate $p^*(-t)$ equals to one. This means that the output of the sample and hold devices can be rewritten in (27).

$$y_h[m] = e^{2\pi j \frac{h}{k}} \sum_{n=1}^{N} \sum_{i=1}^{k} x_{i,n} + z(t) \Big|_{t=mT+\frac{(h-1)T}{k}} \tag{27}$$

This expression can be further simplified by assuming that there is no inter-symbol interference between pulses in the same stream. In this case, although ISI exists between the FTN streams, the pulses within each bit stream are assumed not to interfere with each other at the sampling times. In this case the sum across the *N* symbols for one stream in one packet can be dropped because these symbols will not interfere with each other. Equation (28) shows the simplified version of the output of the sample and hold devices.

$$y_h[m] = \sum_{i=1}^{k} x_{i,n} + z(t)\,|_{t=mT+\frac{(h-1)T}{k}} \tag{28}$$

The output of these the sample and hold circuits is then fed into a soft-decision demodulator. In a physical realization of this receiver, the analog output of the matched filter would be run through a buffer amplifier and the voltage stored in a capacitor long enough for an ADC to make a measurement at time $t=mT+(h-1)T/k$. These digital values would then be sent to the soft decision modulator for further processing. The soft decision is necessary because due to the ISI, a simple threshold device will not be able to accurately decode the received signals.

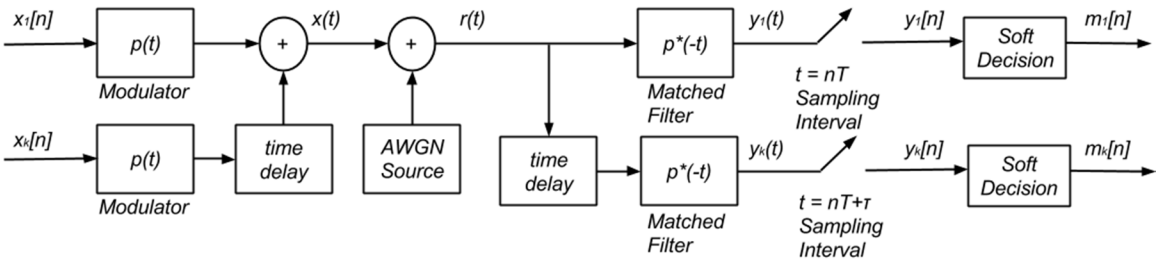

Figure 15. Block diagram of a time domain FTN system with *k* FTN streams

2.3.2 Time-domain Discrete-time FTN Channel Model

The relationship between the inputs and outputs to the time-domain FTN system described in Figure 15 can be also described by a vector equation. The input vector **x** described in (29) takes into account all symbols transmitted in a packet across all FTN streams. This vector contains *kN* entries for the *k* FTN streams and the *N* symbols per FTN stream per packet. In this equation $x_{i,j}$ represents the *j*th symbol on the *i*th FTN streams.

$$\mathbf{x} = \left(x_{1,1}, x_{2,1}, \cdots, x_{k,1}, x_{1,2}, x_{2,2} \cdots x_{k,N} \right) \tag{29}$$

In addition, the output vector **y** can be described by (30). Just as with the equation for the input vector, there are *kN* entries for the *k* FTN streams and the *N* symbols per FTN stream per packet. The entry $y_{i,j}$ represents the *j*th symbol on the *i*th FTN stream.

$$\mathbf{y} = \left(y_{1,1}, y_{2,1}, \cdots, y_{k,1}, y_{1,2}, y_{2,2} \cdots y_{k,N} \right) \tag{30}$$

A channel matrix **H** also exists that describes the correlation between the input and output vectors and is expressed in (31) Unlike the MIMO channel matrix, this channel matrix does not correspond to a physical channel, but provides a way of looking at the input-output relationship over the entire length of the packet.

$$\mathbf{H}_{FTN} = \begin{pmatrix} 1 & h_{-1} & h_{-2} & \cdots & h_{-(kN-1)} \\ h_1 & 1 & h_{-1} & \cdots & h_{-(kN-2)} \\ h_2 & h_1 & 1 & \cdots & h_{-(kN-3)} \\ \vdots & \vdots & \vdots & \ddots & \vdots \\ h_{kN-1} & h_{kN-2} & h_{kN-3} & \cdots & 1 \end{pmatrix} \tag{31}$$

In the expression for **H**, each h_i represents correlation between a pulse *i* and its neighbors at each given sample time. Equation (32) provides a closed form for this correlation with respect the transmitted pulse *i* and the matched filter through which it is passed.

$$h_i = \int_{-\infty}^{\infty} p(\tau - i\frac{T}{k}) p(t-\tau) d\tau |_{t=T} \tag{32}$$

To better visualize this, Figure 16 provides an illustration of the transmitted bits and their respective sampling times for an FTN system with two FTN streams. It can be observed that when the sample and hold device for one stream takes a sample, the sample will also contain some information from an overlapping pulse in another bit stream. The amount of interference depends on the pulse shape and the amount by which each stream is delayed.

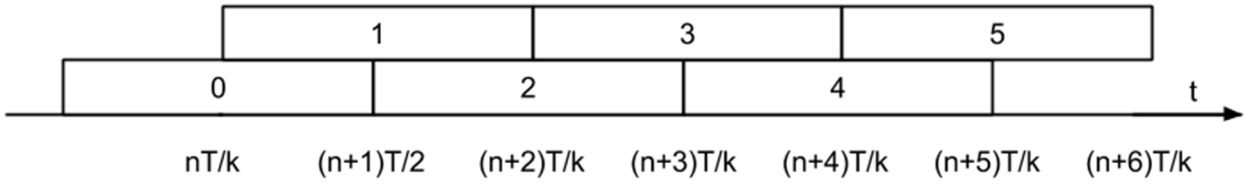

Figure 16. Timing diagram for bits in a *k*=2 FTN system with equal delay between bit streams

The noise covariance matrix $\mathbf{Q_z}$, expressed in (33), is another important attribute of this FTN system.

$$\mathbf{Q}_{Z_{FTN}} = \sigma^2 \mathbf{H}_{FTN} \tag{33}$$

For this system the noise in any given sample is correlated with noise from the surrounding samples. Figure 17 demonstrates this concept that because a single sample also receives power from interfering pulses, it receives their noise as well. Because the noise is additive and occurs before the streams are split, the same noise will appear in different samples at the receiver. The correlation between noise samples will only occur when bits overlap each other in time. The FTN channel matrix provides a map showing which bits overlap each other at any given time in the transmitted packet. This leads to the noise covariance

matrix having the same structure as the channel matrix, but with a magnitude dependent on the noise variance σ^2.

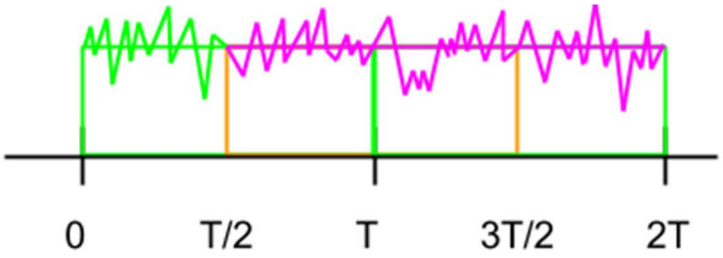

Figure 17. Visualization of noise in an FTN system: the purple waveform represents the combination of noise from the orange and green bits where they overlap in time

2.4. Capacity of FTN Systems

Using the FTN system described in Section 2.3, an upper bound for the system's capacity can be calculated. This section will derive a general equation for the capacity of this type of FTN system and provide a comparison of the capacities of FTN systems with different FTN rates *k*.

2.4.1 Derivation of the FTN Capacity Formula

A derivation of the Capacity Formula for the time domain FTN system described in Figure 15 was made by Kim in [29]. This section closely follows this derivation but with different notation to accommodate the capacity formula of the combined FTN MIMO system presented in the next chapter. Just as with the MIMO system, the capacity of an FTN system can be derived starting with the Shannon capacity formula in (34). However, unlike the MIMO capacity equation which considers the capacity of a single channel use, the

capacity of an entire transmitted packet is considered. Thus the mutual information must be normalized by the length of the packet, 1/*N*, to obtain the capacity per channel use. The normalization does not include the FTN factor *k* because the extra FTN streams add a negligible length to the end of a packet for large packet sizes. The effects of the extra streams will be taken into account by the power in each pulse sent from the transmitter.

$$C = \max_{p(\mathbf{X})} \left(\frac{1}{N} I(\mathbf{X};\mathbf{Y}) \right) = \max_{p(\mathbf{X})} \left[\frac{1}{N} (H(\mathbf{Y}) - H(\mathbf{Y} \mid \mathbf{X})) \right] \tag{34}$$

Once again the entropy **Y** is defined in (35) and the entropy of **Y** given **X** is defined in (36). The entropies are defined across the entire input vector **x** and the entire output vector **y**. Just as in the MIMO capacity derivation, H(**Y**|**X**) is equal to the entropy of the noise H(**z**).

The covariance of the received signal vector $\mathbf{Q_y}$ can be determined using (37) if the covariance matrix of the transmitted signal $\mathbf{Q_x}$ is known as well as the noise covariance matrix $\mathbf{Q_z}$.

$$\mathbf{Q}_\mathbf{y} = \mathbf{H}\mathbf{Q}_\mathbf{x}\mathbf{H}^H + \mathbf{Q}_\mathbf{z} \tag{37}$$

This means that the capacity can be determined based on the vectorized channel model. Equation (38) shows the preliminary form of this equation.

$$C = \log_2(\det(\mathbf{H}\mathbf{Q}_\mathbf{x}\mathbf{H}^* + \mathbf{Q}_\mathbf{z})) - \log_2(\det(\mathbf{Q}_\mathbf{z})) \tag{38}$$

For FTN systems with the receiver structure shown in Figure 15, the noise covariance matrix can be expressed as $\sigma^2\mathbf{H}$ where σ^2 is the noise variance. This can be substituted into the expression shown in (39).

$$C = \log_2\left(\frac{\det(\mathbf{H}\mathbf{Q}_x\mathbf{H}^* + \sigma^2\mathbf{H})}{\det(\sigma^2\mathbf{H})}\right) \tag{39}$$

Further algebraic manipulations allows the capacity to be expressed by (40).

$$C = \log_2\left(\det\left(\mathbf{I}_{kN} + \frac{\mathbf{H}\mathbf{Q}_x}{\sigma^2}\right)\right) \tag{40}$$

If the transmitter is making no attempt to precode the transmitted signal and the transmitted symbols are independent, then the covariance matrix of the transmitted signal $\mathbf{Q}_x$ can be expressed as $\mathbf{I}_{kN}$, a square identity matrix of size kN. The expression for $\mathbf{Q}_x$ can be plugged back into the expression for capacity of an FTN system to yield the final form of the FTN capacity formula for the aforementioned receiver architecture.

$$C = \frac{1}{N}\log_2\left(\det\left(\mathbf{I}_{kN} + \frac{1}{\sigma^2}\mathbf{H}\right)\right) \tag{41}$$

2.4.2 FTN Capacity Results

Figure 18 shows the capacity of various FTN systems compared to that of a Nyquist rate system using the rectangular pulse shape. The rectangular pulse is defined in equation (42). In a Nyquist rate system, a pulse rectangular pulse with unit energy would have an amplitude of $1/\sqrt{T}$. However, in an FTN system, additional pulses are being transmitted at the same time. In order to ensure that the transmitter is sending the same power as in the Nyquist rate case, a further normalization factor of $1/\sqrt{k}$ is needed. Thus at any given time instant, the sum of the power from each transmitted pulse cannot exceed the power in a single transmitted pulse from the Nyquist rate system.

$$p(t) = 1/\sqrt{kT} \text{ for } 0 \le t < T \tag{42}$$

Using the pulse shape defined above, the channel matrix **H** for an FTN system with k streams can be expressed in (43).

$$\mathbf{H}_{FTN} = \frac{1}{\sqrt{k}} \begin{pmatrix} 1 & \max\left(\frac{k-1}{k},0\right) & \max\left(\frac{k-2}{k},0\right) & \cdots & 0 \\ \max\left(\frac{k-1}{k},0\right) & 1 & \max\left(\frac{k-1}{k},0\right) & \cdots & 0 \\ \max\left(\frac{k-2}{k},0\right) & \max\left(\frac{k-1}{k},0\right) & 1 & \cdots & 0 \\ \vdots & \vdots & \vdots & \ddots & \vdots \\ 0 & 0 & 0 & \cdots & 1 \end{pmatrix} \tag{43}$$

It can be observed that FTN leads to an increase in capacity for a given bandwidth, particularly at higher SNRs. It can also be observed that FTN suffers from diminishing returns; as the Nyquist rate is violated by greater amounts, the capacity gains are not as great the capacity gain from no FTN to 2xFTN signaling.

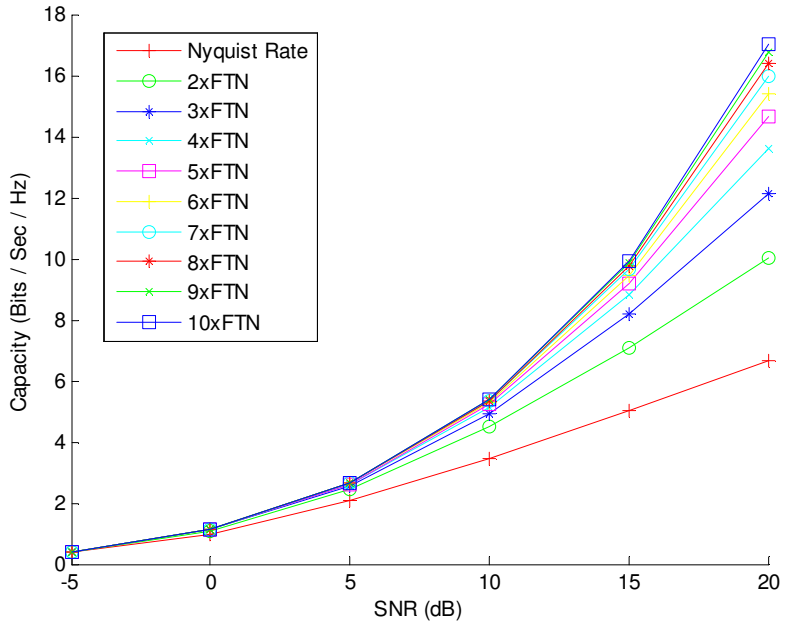

Figure 18. Capacities of FTN systems from k=1…10

2.5. Relative Merits of MIMO and FTN Systems

The complexity of both FTN and MIMO transmitters and receivers increases linearly with the number of antennas or FTN streams. Based on the results in the previous sections, it can be observed that if both the number of transmit and receive antennas is increased in a MIMO system, the capacity gain will be greater than that of an FTN system with the corresponding number of FTN streams. For example, a 10x10 MIMO system will yield a greater capacity than a 10xFTN system. This is particularly true at lower SNRs where the MIMO system performs well in terms of capacity when compared with the corresponding FTN system, particularly if the MIMO system is able to use CSIT.

However, there are some situations where MIMO would not be appropriate due to size constraints on a physical device coupled with the need to space antennas far enough apart to achieve sufficient multipath fading. Thus, even though a 10x10 MIMO shares the same complexity as a 10xFTN system and outperforms it in terms of channel capacity, it may not always be feasible to implement compared to the FTN system.

Chapter 3. FTN MIMO with CSIR and CSIT

In this chapter several models are put forward for a combined FTN MIMO receiver. The ergodic channel capacity is derived and the results presented graphically. The derivation follows the channel capacity derivation from [1], which was originally determined by Yi Feng. Both cases where channel knowledge is only available at the receiver and channel knowledge is available at both the transmitter and receiver are considered.

3.1. FTN MIMO Combined Receiver Architecture

Figure 19 shows the basic FTN MIMO combined system architecture that was put forward in [1]. This intuitive combined FTN MIMO architecture involves simply generating k FTN streams at each transmit antenna and then sending these kNn_t FTN streams across a MIMO channel to a receiver. At each transmit antenna, the transmitted waveform reflects that of a standard FTN transmitter as described in (44).

$$x_j(t) = \sum_{n=1}^{N}\sum_{m=1}^{k} \frac{1}{\sqrt{n_T k}} x_{j,n,m} p(t-(n-1)T - \frac{T(m-1)}{k}) \tag{44}$$

In this case, $x_j(t)$ is the continuous time transmitted signal from the jth antenna at time t. The variable $x_{j,n,m}$ corresponds to the symbol transmitted from the jth transmitting antenna in the nth time position in the packet on the mth FTN stream. In this case the packet is of length kn_tN where N is the number of symbols in one FTN stream. The modulating pulse

p(t) is unit energy. In order to correct for n_t extra antennas and *k* extra FTN streams, the modulating pulse is normalized by $1/\sqrt{n_t k}$ so that the total power transmitted at any given time does not exceed the power for a SISO, Nyquist rate communication system using a unit energy pulse. The signal recovered at the *i*th receiving antenna, $r_i(t)$, is described below.

$$r_i(t) = \sum_{j=1}^{n_T} \sum_{n=1}^{N} \sum_{m=1}^{k} \frac{1}{\sqrt{n_T k}} h_{i,j} x_{j,n,m} p(t-(n-1)T - \frac{T(m-1)}{k}) + z_i(t) \tag{45}$$

At each receiving antenna, the sum of signals from each transmitting antenna $1 \ldots n_t$ are recovered with each attenuated by some factor $h_{i,j}$, which corresponds to the gain between the *i*th receiving antenna and the *j*th transmitting antenna. Depending on the MIMO channel model used, this gain can be complex. In addition, AWGN is added in the receiver circuitry in the analog signal chain for each receiving antenna. The AWGN is independent between receiving antennas and the noise added to received signal waveform on the *i*th receive antenna at time *t* is described by $z_i(t)$. The spectral density of the AWGN at each signal chain is assumed to be $N_0/2$. At each signal chain, the signal $r_i(t)$ is split into *k* copies for each FTN stream. The *m*th copy at each antenna is delayed by $(m-1)/T$ seconds. After this delay, the signal copies are passed through a matched filter with an impulse response $p^*(-t)$. The continuous time signal $y_{i,m}(t)$ below describes the signal at the output of the matched filter for the *m*th FTN stream on the *i*th receive antenna.

$$y_{i,m}(t) = \int_{-\infty}^{\infty} r_i(\tau - \frac{m-1}{T}) p^*(t+\tau) d\tau \tag{46}$$

After matched filtering, each signal $y_{i,m}(t)$ is passed through a sampling device. The devices are sampled periodically every T seconds to obtain the discrete time signal $y_{i,m}[n]$ on the ith receive antenna for the mth FTN stream.

$$y_{i,m}[n] = y_{i,m}(t)|_{t=nT} \tag{47}$$

The samples are then passed to a soft decision decoder capable of reconstructing the transmitted data given knowledge of the MIMO channel and the attributes of the FTN system such as number of streams, pulse shape, and delay between streams. A likely candidate for the soft decision decoder would be a Viterbi decoder, but because this receiver has correlated noise, it is unknown if a Viterbi decoder is the optimal soft decision decoder. It is also important to note that this receiver structure is very sensitive jitter and timing errors between the transmitter and receiver. One method of compensating for these is to add an equalizer at the input of the receiver or utilize the Viterbi decoder to try and compensate for errors caused by jitter. Because of this added complexity, this system would likely be more applicable on the uplink channel where a mobile device with constrained battery and processing power only has to add transmitted signal streams together, while a base station with access to more electrical and processing power would be able to perform the decoding of the transmitted message.

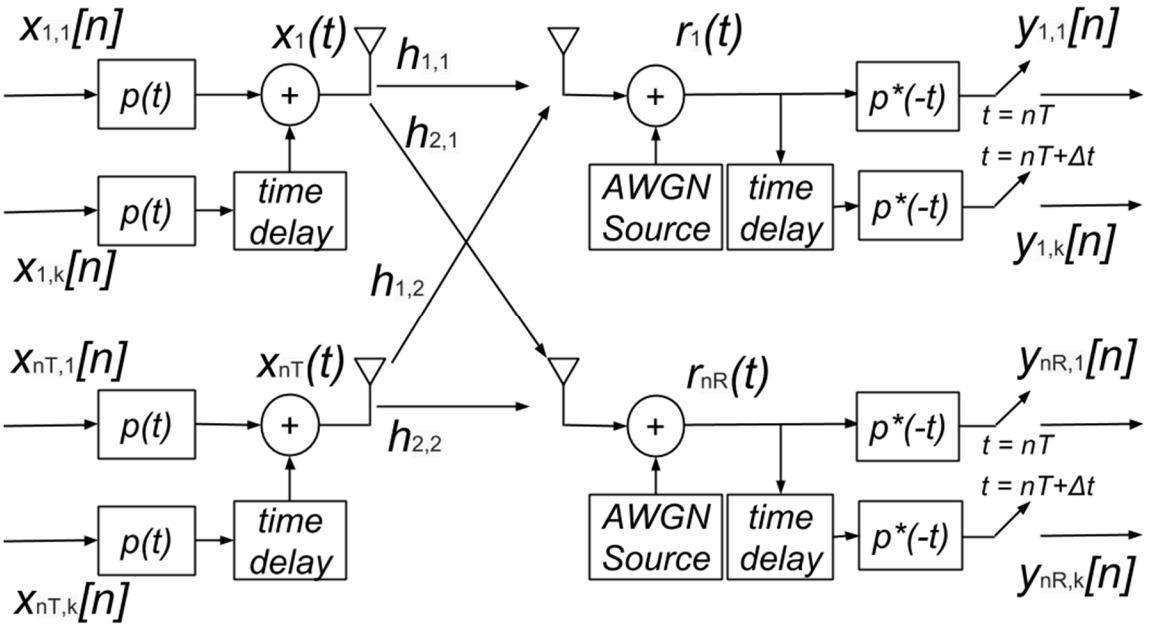

Figure 19. Block Diagram of an FTN MIMO system with $n_T = n_R = 2$ and $k=2$

The relation between the inputs and the outputs to the FTN MIMO system can also be described by the vector equation **y=Hx+z**. In this case, the input vector **x** of size $n_T kN$ is shown in (48).

$$\mathbf{x} = \left(x_{1,1,1}\, x_{1,1,2} \ldots\ x_{1,1,k}\, x_{1,2,1}\, x_{1,2,2} \ldots\ x_{1,N,k}\, x_{2,1,1}\, x_{2,1,2} \ldots\ x_{n_T,N,k} \right)^T \tag{48}$$

Furthermore, the output vector **y** can be written as a vector as shown in (49). The received signal vector is size $n_R kN$

$$\mathbf{y} = \left(y_{1,1}[1]\, y_{1,2}[1] \ldots y_{1,k}[1]\, y_{1,1}[2]\, y_{1,2}[2] \ldots y_{1,k}[N]\, y_{2,1}[1]\, y_{2,2}[1] \ldots y_{n_{T_R},k}[N] \right)^T \tag{49}$$

The AWGN is represented by the vector **z**, which must be of the same dimensions as the output vector **y**. Each entry $z_{i,n,m}$ corresponds to the additive noise on the nth sample of the mth FTN stream on the ith receive antenna. Each entry is a zero mean Gaussian

random variable with variance σ^2. In an AWGN process, the variance is equal to the power spectral density $N_0/2$.

$$\mathbf{z} = \left(z_{1,1,1}\ z_{1,1,2} \cdots\ z_{1,1,k}\ z_{1,2,1}\ z_{1,2,2} \cdots\ z_{1,N,k}\ z_{2,1,1}\ z_{2,1,2} \cdots\ z_{n_R,N,k} \right)^T \tag{50}$$

The channel matrix $\mathbf{H}$ is an $n_T kN$ by $n_R kN$ matrix that represents the relation between each channel input and output. Because the input and output vectors are both defined in such a way that there is a block of entries for each antenna with kN entries to represent the kN symbols transmitted per packet at that antenna, the channel matrix can be represented as a kronecker product of the FTN and MIMO channel matrices defined in Chapter 2.

$$\mathbf{H}_{FTN-MIMO} = \mathbf{H}_{MIMO} \otimes \mathbf{H}_{FTN} \tag{51}$$

$$\mathbf{H}_{FTN-MIMO} = \begin{pmatrix} h_{1,1}\mathbf{H}_{FTN} & \cdots & h_{1,n_T}\mathbf{H}_{FTN} \\ \vdots & \ddots & \vdots \\ h_{n_R,1}\mathbf{H}_{FTN} & \cdots & h_{n_R,n_T}\mathbf{H}_{FTN} \end{pmatrix} \tag{52}$$

Just as in MIMO and FTN systems, the covariance matrix of the noise and input vectors also needs to be considered. The noise covariance matrix follows a similar pattern as the FTN channel matrix in that it is made up of blocks representing each antenna; the blocks are kN by kN and contain information about the covariance between symbols in each FTN stream. Equation (53) shows the noise covariance matrix $\mathbf{Q_z}$ as the kronecker product of the noise covariance matrix of the FTN and MIMO systems scaled by $1/\sigma^2$ so that the noise variance is not accounted for twice after the kronecker product.

$$\mathbf{Q}_{Z_{FTN-MIMO}} = \frac{1}{\sigma^2}\mathbf{Q}_{Z_{MIMO}} \otimes \mathbf{Q}_{Z_{FTN}} \tag{53}$$

Note that for the MIMO receiver the noise covariance matrix is simply $\sigma^2\mathbf{I}_{n_R}$ and for FTN the noise covariance matrix is $\sigma^2\mathbf{H}_{FTN}$. Thus, for the system depicted in Figure 19, the noise covariance matrix can be expressed by (54). Note that there is correlation between noise on the samples at the same antenna, but no correlation in noise for samples from different antennas.

$$\mathbf{Q}_{Z_{FTN-MIMO}} = \begin{pmatrix} \sigma^2\mathbf{H}_{FTN} & 0 & \cdots & 0 \\ 0 & \sigma^2\mathbf{H}_{FTN} & \cdots & 0 \\ \vdots & & \ddots & 0 \\ 0 & \cdots & 0 & \sigma^2\mathbf{H}_{FTN} \end{pmatrix} \tag{54}$$

Also of interest is $\mathbf{Q_x}$, the input covariance matrix. In this system it is assumed that there is no CSI at the transmitter, so the best the transmitter can do is to transmit iid symbols. Because of that the the input covariance matrix is an identity matrix of size $n_T kN$.

3.2. Ergodic Capacity of the Basic FTN MIMO Receiver

Just as with the FTN and MIMO systems, the Shannon capacity of the FTN MIMO system can be derived starting with the mutual information between the transmitter and the receiver. The mutual information can be written as the difference between the entropy in the received signal and $H(\mathbf{Y}|\mathbf{X})$, which is equal to the entropy of the noise $H(\mathbf{z})$. Because an entire packet is being considered, the mutual information between the transmitter and receiver must be divided by the length of one FTN stream on one antenna to obtain the capacity per channel use.

$$C = \max_{p(\mathbf{X})}\left(\frac{1}{N} I(\mathbf{X};\mathbf{Y})\right) = \max_{p(\mathbf{X})}\left[\frac{1}{N}(H(\mathbf{Y}) - H(\mathbf{Y}\mid\mathbf{X}))\right] \tag{55}$$

The entropies can be rewritten as expressions involving the covariance matrices received signal vector and the noise signal vector.

$$C = \frac{1}{N}\left(\log_2(\det(\mathbf{Q}_\mathbf{y})) - \log_2(\det(\mathbf{Q}_\mathbf{z}))\right) \tag{56}$$

Just as with FTN and MIMO, the covariance matrix of the received signal can be expressed by (57).

$$\mathbf{Q}_\mathbf{y} = \mathbf{H}\mathbf{Q}_\mathbf{x}\mathbf{H}^H + \mathbf{Q}_\mathbf{z} \tag{57}$$

This can be substituted into the expression for capacity to yield equation (58).

$$C = \frac{1}{N}\left(\log_2(\det(\mathbf{H}\mathbf{Q}_\mathbf{x}\mathbf{H}^* + \mathbf{Q}_\mathbf{z})) - \log_2(\det(\mathbf{Q}_\mathbf{z}))\right) \tag{58}$$

This expression for the capacity can be rewritten as the log of a division of determinants to give the final form of the capacity equation shown in equation (59).

$$C = \frac{1}{N}\log_2 \frac{\det\left(\mathbf{H}_{FTN-MIMO}\mathbf{Q}_x\mathbf{H}^*_{FTN-MIMO} + \mathbf{Q}_{z_{FTN-MIMO}}\right)}{\det\left(\mathbf{Q}_{z_{FTN-MIMO}}\right)} \tag{59}$$

However, this capacity equation only represents the capacity of one realization of the MIMO channel matrix. To determine the average capacity that can be achieved with many different MIMO channel matrices, the expected value of the capacity over many channel realizations must be considered. This is called ergodic capacity and can be expressed in (60).

$$C = E_{\mathbf{H}_{FTN-MIMO}}\left(\frac{1}{N}\log_2 \frac{\det\left(\mathbf{H}_{FTN-MIMO}\mathbf{Q}_x\mathbf{H}^*_{FTN-MIMO} + \mathbf{Q}_{z_{FTN-MIMO}}\right)}{\det\left(\mathbf{Q}_{z_{FTN-MIMO}}\right)}\right) \tag{60}$$

Using this ergodic capacity expression, the Shannon capacity for various FTN MIMO systems was evaluated and compared. All the subsequent graphs use a square pulse normalized to the number of transmitting antennas and FTN streams as shown in (61). The square pulse shape was selected because of its use in Wi-Fi. Other common pulses include root-raised cosine, which is a potential subject for future research.

$$p(t) = 1/\sqrt{n_T kT} \text{ for } 0 \le t < T \tag{61}$$

In this thesis, the ergodic capacity is evaluated by averaging over one thousand realizations of the channel matrix. One thousand realizations was selected because beyond this number, the fluctuation in average observed capacity is insignificant.

Figure 20 supposes that FTN is added to a 2x2 MIMO system. It shows the capacity increase for various FTN rates for the SNR ranging from -5dB to 20dB. It can be observed that adding FTN to the MIMO system causes an increase in capacity. This makes sense because the rank of the kronecker product of two matrices will always be the product of the ranks of those two matrices. Thus the number of parallel Gaussian channels that come from the FTN MIMO channel matrix is the product of those of the MIMO and FTN systems.

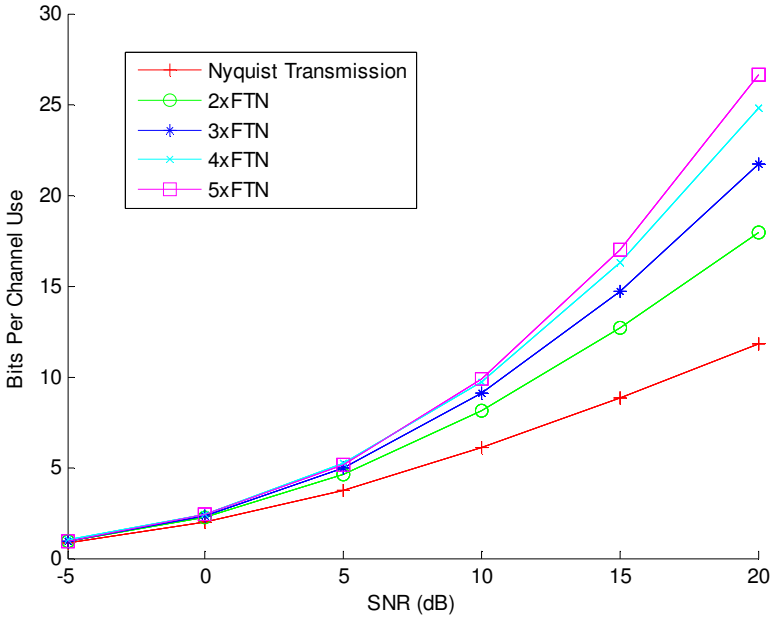

Figure 20. Capacity of a 2x2 MIMO System with FTN rates k=1…5

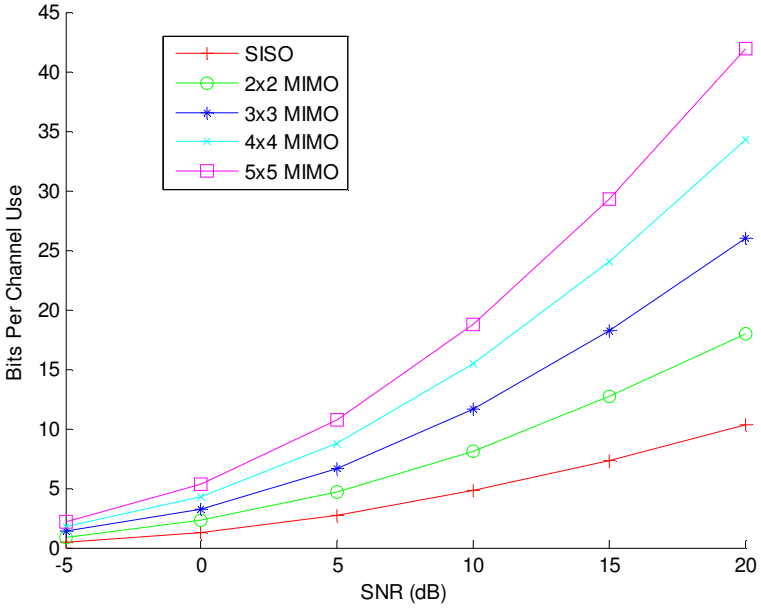

Figure 21. Capacities of a 2xFTN system for various MIMO configurations

Figure 21 supposes that MIMO is added to a 2xFTN system. It looks at the effects of symmetric MIMO (where the number of transmitting antennas equals the number of receiving antennas) from 2x2 MIMO to 5x5 MIMO across SNRs from -5dB to 20dB. It can be observed that the addition of MIMO also causes the capacity to increase for all SNRs.

Figure 22 shows the capacity effect of varying FTN rates on an *N*x*N* MIMO system for *N* from 1 to 6. It can be observed that adding FTN to any of these MIMO systems leads to an increase in capacity, however diminishing returns are experienced as more and more FTN streams are added.

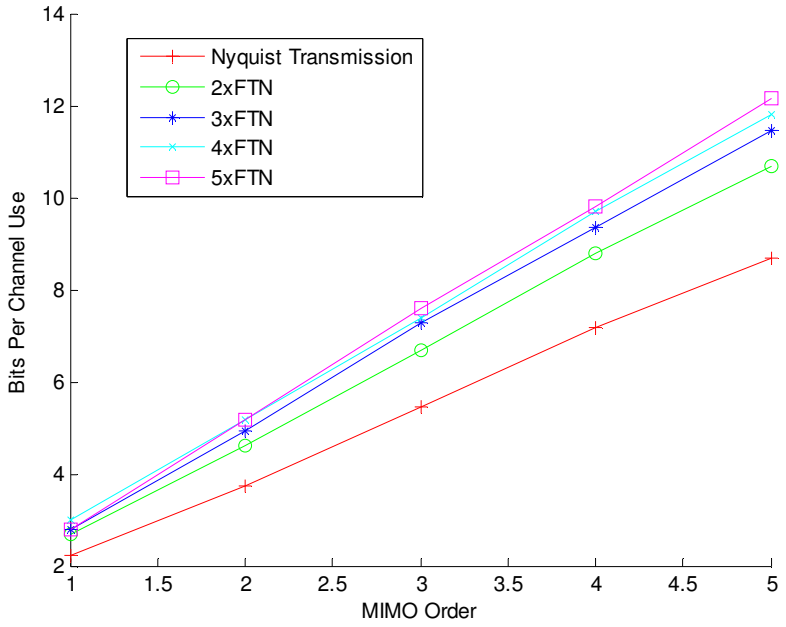

Figure 22. Comparison of systems with varying FTN and MIMO configurations at 5dB

Figure 23 supposes that FTN is added to a 2x1 MIMO system. It shows the capacity increase for various FTN rates across SNRs from -5dB to 20dB. It can be observed that

adding FTN to the MIMO system causes an increase in capacity, though not as much as in the case of the symmetric MIMO system. Nevertheless, this is interesting because in the case of a system with more transmitters than receivers, adding more transmitting antennas does little to improve the capacity. This graph highly suggests that the capacity can be improved by adding FTN to this kind of an asymmetric MIMO.

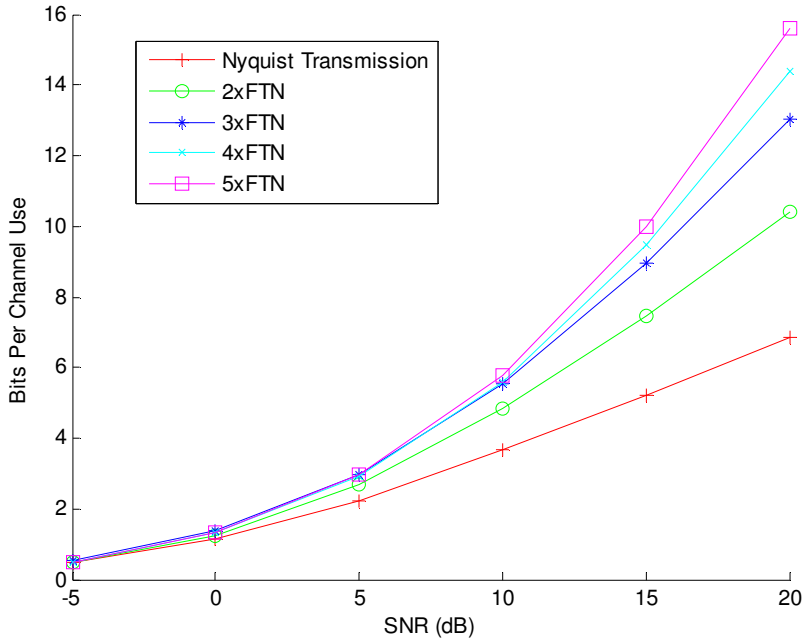

Figure 23. Capacity of a 2x1 MIMO system with FTN rates *k*=1…5

Figure 24 supposes that MIMO with more transmitters than receivers is added to a 2xFTN system. It looks at the effects of asymmetric MIMO from 2x1 to 5x1 systems across SNRs from -5dB to 20dB. It can be observed that the addition of MIMO only leads to a negligible capacity gain, just as MIMO with more transmit than receive antennas and CSIR only leads to a negligible capacity gain in a Nyquist rate system.

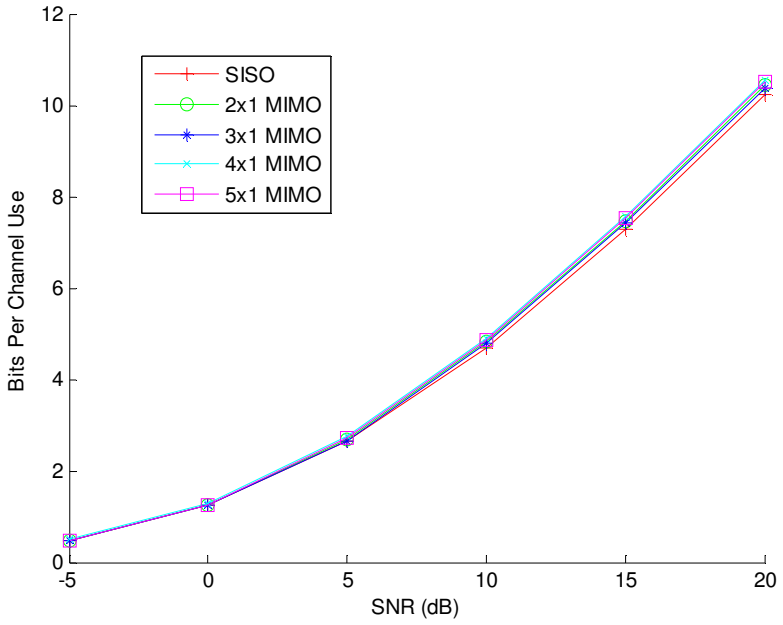

Figure 24. Capacity of a 2xFTN system with various MIMO configurations

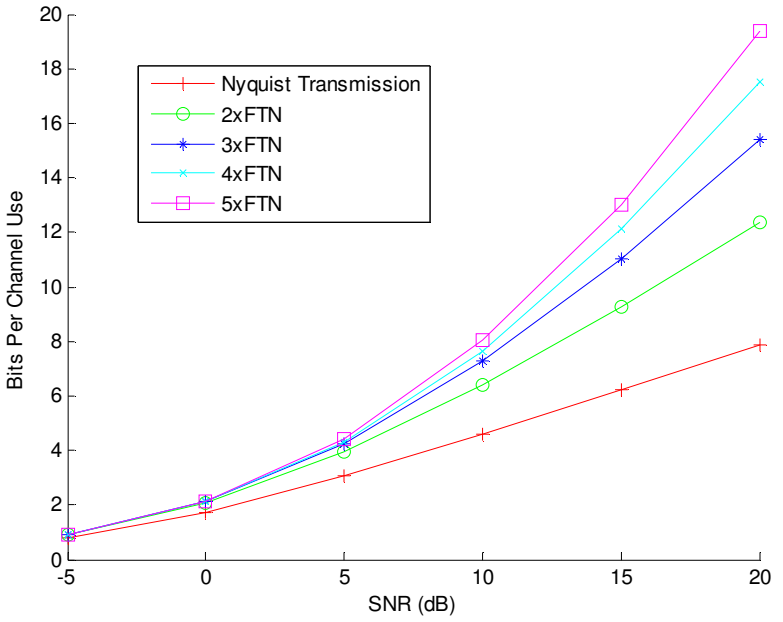

Figure 25. Capacity of a 1x2 MIMO system with FTN rates k=1…5

Figure 25 supposes that FTN is added to a 1x2 MIMO system. It shows the capacity increase for various FTN rates from -5dB to 20dB SNR. It can be observed that adding FTN to the MIMO system causes an increase in capacity, though not as much as in the case of the symmetric MIMO system. However, the capacity gain is higher than the case where there are more transmitting antennas than receiving antennas.

Figure 26 supposes that MIMO with more receiving antennas than transmitting antennas is added to a 2xFTN system. It looks at the effects of asymmetric MIMO from 1x2 to 1x5 systems across SNRs from -5dB to 20dB. It can be observed that the addition of MIMO leads to a capacity gain, particularly at lower SNRs, just as in the Nyquist rate case for MIMO systems with more receiving antennas than transmitting antennas.

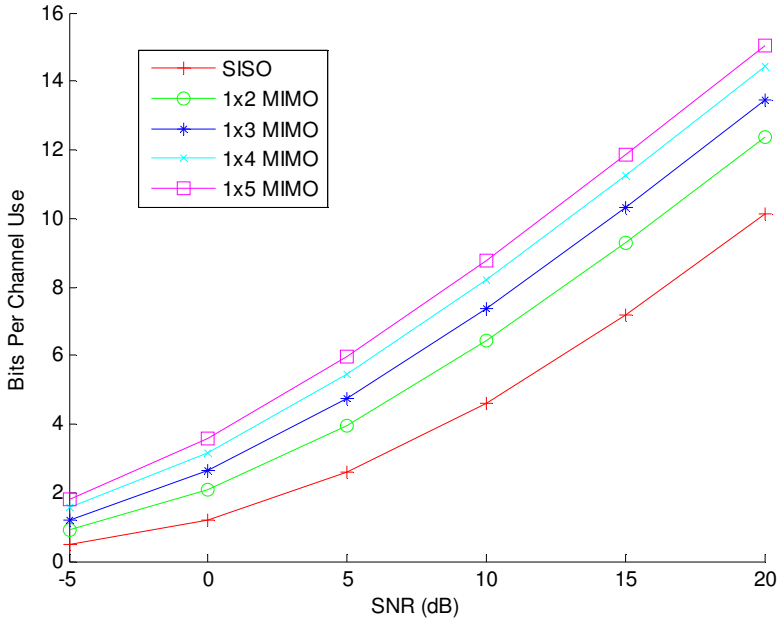

Figure 26. Capacity of an 2xFTN system with various MIMO configurations

Figure 27 shows the capacity of various FTN and MIMO systems for symmetric MIMO. It can be observed that all systems outperform the SISO Nyquist rate system in terms of capacity. The 2x2 MIMO system is superior to the 2xFTN system in terms of capacity for the SNR range analyzed, but the 2xFTN system shows a more rapid increase in capacity at higher SNRs. However, by combining the FTN and MIMO systems, a capacity is achieved that outperforms all the other analyzed systems.

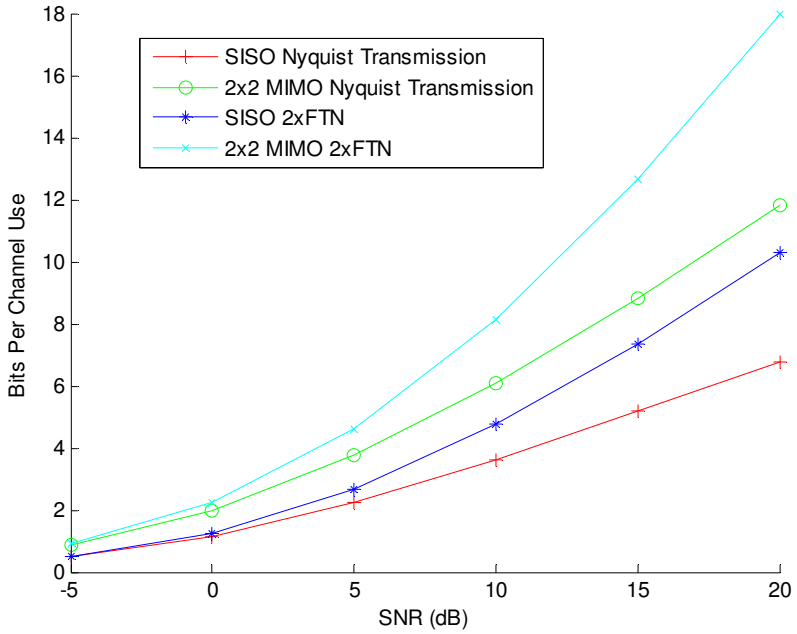

Figure 27. Capacity comparison of a SISO Nyquist rate system, 2x2 MIMO Nyquist rate system, SISO 2xFTN system, and a 2x2 MIMO 2xFTN System

Figure 28 shows the capacity of various FTN and MIMO systems when the MIMO system has more transmitting antennas than receiving antennas. The 2x1 MIMO system with no FTN and the SISO system with no FTN perform similarly in terms of capacity. Similarly, the SISO 2xFTN system and the 2x1 MIMO 2xFTN system also perform

similarly. This would indicate that there is not much capacity gain by increasing the number of transmitting antennas without also increasing the number of receiving antennas. However, it also indicates that adding FTN to an existing 2x1 MIMO system would lead to large capacity gains.

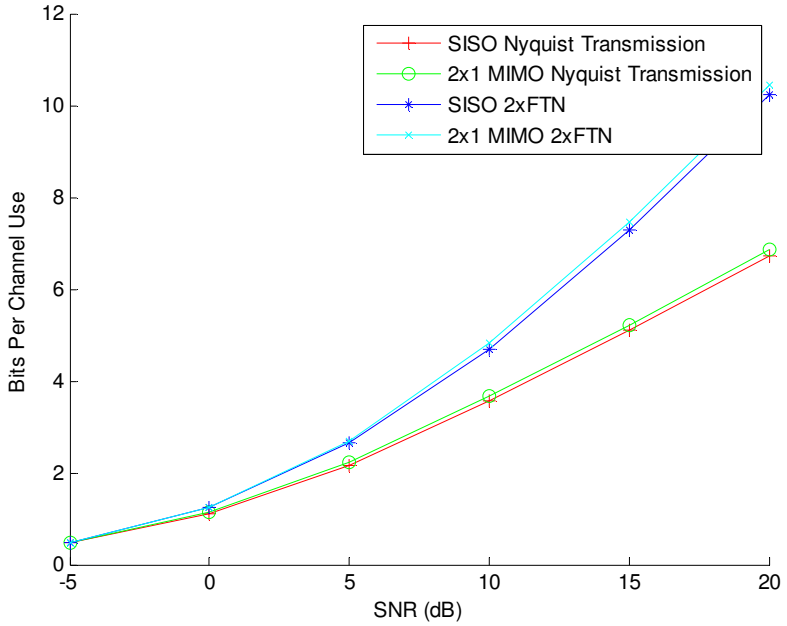

Figure 28. Capacity comparison of a SISO Nyquist rate system, a 2x1 MIMO Nyquist rate system, a SISO 2xFTN system, and a 2x1 MIMO 2xFTN system

Figure 29 shows the capacity of various FTN and MIMO systems when the MIMO system has more receiving antennas than transmitting antennas. It can be observed that all systems outperform the SISO Nyquist rate system. The 1x2 MIMO system with no FTN outperforms the SISO 2xFTN system at low SNRs but for SNRs greater than 10dB, the SISO 2xFTN system has a better capacity. The 1x2 MIMO 2xFTN system outperforms all the other systems.

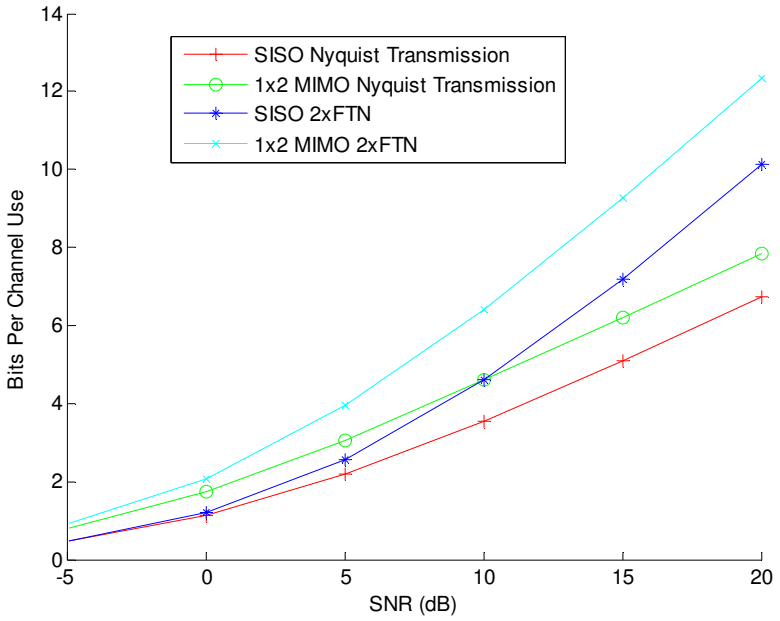

Figure 29. Capacity comparison of a SISO Nyquist rate system, a 1x2 MIMO Nyquist rate system, a SISO 2xFTN system, and a 1x2 MIMO 2xFTN system

The results presented above show that in general, increasing the dimensionality of the FTN MIMO system leads to an increase in channel capacity. It is interesting to note that adding FTN to a MIMO system with a fixed number of receiver antennas allows for an improvement in channel capacity at higher SNRs even though a MIMO system with this same antenna configuration would not experience such improvements with Nyquist rate signaling.

3.3. Orthogonalized FTN MIMO Receiver Architecture

In Section 3.1, an FTN MIMO system was constructed by simply transmitting and receiving k FTN streams independently at each antenna. The architecture was a simple

combination of the existing FTN and MIMO architectures. Although the transmitter architecture is relatively easy to implement in hardware, the receiver requires $n_R k$ matched filters and sampling devices. Furthermore, there is correlated noise at the receiver which makes designing an optimal decoder non-trivial. To combat these issues, the orthogonalized FTN MIMO receiver architecture from [1] is introduced in Figure 30. This architecture only requires one matched filter and sampling device per receive antenna. Furthermore, it will be shown that the noise of the received signal is uncorrelated. The major drawbacks of this new architecture are that the sampling device must now be k times faster than previously required and only rectangular pulses can be used with this system.

The system described in Figure 30 has the same transmitter architecture and channel model as the FTN MIMO system described in the previous section. Thus the equation describing the transmitted signal at the jth antenna $x_j(t)$ is still described by (44) in Section 3.1 and the equation for the received signal $r_i(t)$ at the ith antenna after AWGN is added in the receiver amplifier circuits is still described by (45) in Section 3.1. In this system, however, the received signal is passed through a single filter with impulse response $\varphi(t)$. This means the output of the filter on the ith receive antenna $y_i(t)$ can be described by (62).

$$y_i(t) = \int_{-\infty}^{\infty} r_i(\tau)\phi(t-\tau)d\tau \tag{62}$$

After the filter, the signal $y_i(t)$ is then sampled at intervals of T/k seconds. This is a single sampling device operating at k times the sampling rate of a Nyquist rate system. Thus the system output at time n at the ith receive antenna is shown in (63).

$$y_i[n] = y_i(t)\Big|_{t=\frac{nT}{k}} \tag{63}$$

The system output from each antenna $y_i[n]$ is then passed to a soft decision demodulator. The soft decision demodulator is necessary because the recovered samples do not directly correspond to transmitted symbols, but must be decoded in order to determine the transmitted message.

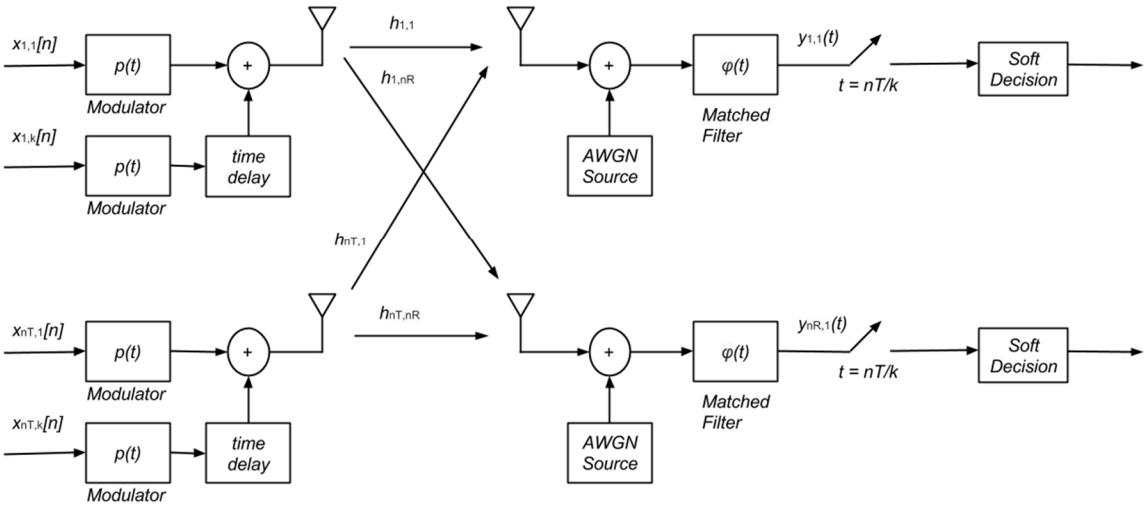

Figure 30. Block diagram of an orthogonalized FTN MIMO system (Note that $\varphi(t)$ is not matched to the input pulse $p(t)$)

In this alternative FTN receiver architecture, the pulse shape $p(t)$ and the receiver filter impulse response $\varphi(t)$ must be carefully selected. Because of the sampling period of T/k, $\varphi(t)$ must be selected so that is has zero amplitude at all times nT/k for all n except 0 to avoid introducing ISI at the filter. The goal is that the convolution of the filter pulse and the transmitted pulse on any interval $[0,T/k),[T/k,2T/k),\ldots[(k-1)T/k,T)$ should be equal. The only way to accomplish this with the system diagram in Figure 30 is to select a

rectangular pulse for *p(t)* with support [0,*T*) and a rectangular pulse for $\varphi(t)$ with support [0,*T/k*). In the subsequent capacity calculations, the normalization for number of antennas and FTN streams will be applied to the transmitted pulse *p(t)*. The filter pulse $\varphi(t)$ must therefore be unit energy to avoid interfering with this normalization. Because $\varphi(t)$ is only defined on the interval [0,*T/k*), it can be defined by (64) for a system with *k* FTN streams and transmit pulse period *T*.

$$\phi(t) = \frac{\sqrt{k}}{\sqrt{T}} \text{ for } 0 \le t < \frac{T}{k} \tag{64}$$

Just as in the previous sections, the relationship between the inputs and outputs of this system can be described by a vector equation **y=Hx+z**. Because the transmitter structure is the same, the transmit vector **x** remains the same as in (48). Now however, the received vector **y** is no longer a list of samples corresponding to individual transmitted symbols, but a list of all samples at the output of the sampling device. Equation (65) provides an expression for **y**. It is important to note that even though each sample does not correspond exactly with a transmitted symbol, the information across all received samples can be decoded using a trellis to determine the original transmitted symbols.

$$\mathbf{y} = \left(y_1[1]\ y_1[2]\ y_1[3] \cdots y_1[kN+k-1]\ y_2[1]\ y_2[2] \cdots y_{n_T}[kN+k-1] \right)^T \tag{65}$$

Just as in the FTN MIMO system described in Section 3.1, each received sample contains additive noise. In this case the noise vector **z** can be written as in (66) where each entry $z_{i,j}$ corresponds to the noise added to the *j*th sample on the *i*th receive antenna. Each entry is a zero-mean Gaussian random variable with variance σ^2. However, in this system,

each entry in the noise vector is uncorrelated because there is no overlap in the received samples as in the traditional FTN receiver architecture.

$$\mathbf{z} = \left(z_{1,1}\ z_{1,2}\ z_{1,3} \cdots z_{1,kN+k-1}\ z_{2,1}\ z_{2,2} \cdots z_{n_T,kN+k-1} \right)^T \tag{66}$$

The channel matrix for this system also shows the relation between each input symbol to the system and each output sample. Just as in Section 3.1, the FTN MIMO channel matrix can be written as a kronecker product of the FTN and MIMO channel matrices. Now, however, the FTN channel matrix has changed form because of the new receiver structure introduced to detect FTN streams. In general, a channel matrix **H** can be written such that each entry $h_{i,j}$ denotes the correlation between the ith transmitted symbol and the jth received sample. Because transmitted symbols can only interfere with up to $2k$ neighboring pulses, the channel matrix structure for this orthogonalized FTN receiver can be generalized as in (67). Note that kN symbols were transmitted, but $kN+k-1$ samples are received causing the channel matrix to be size kN by $kN+k-1$. After the last transmitted symbol on the first FTN stream, the receiver can still gather still k-1 samples to collect data from the transmitted waveform.

$$\mathbf{H}_{FTN_{OS}} = \begin{pmatrix} h_0 & h_{-1} & \cdots & h_{kN+k-2} \\ h_1 & h_0 & \cdots & h_{kN+k-3} \\ h_2 & h_1 & \cdots & h_{kN+k-4} \\ \vdots & h_2 & \cdots & h_{kN+k-5} \\ \vdots & \vdots & \ddots & \vdots \\ h_{kN+k-2} & h_{kN+k-3} & \cdots & h_0 \end{pmatrix} \tag{67}$$

Figure 31 helps to visualize where the extra received samples originate by showing the sampling times for a 2xFTN system. In this figure the black rectangles refer to

independent symbols numbered in blue from zero to five. The red lines and numbers correspond to each sample that the receiver will take in relation to the transmitted symbols. In this case, the FTN channel matrix would have dimensions 6 by 7.

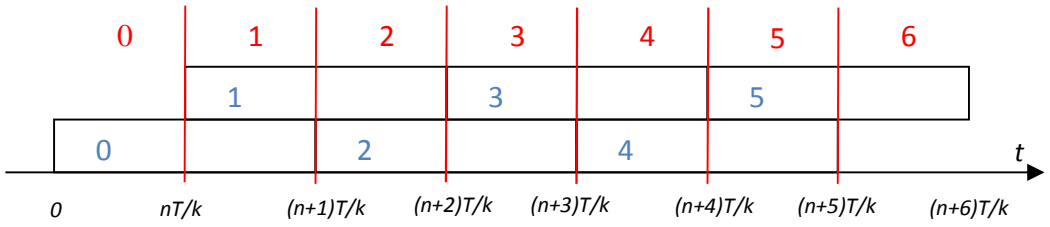

Figure 31. Sample times and their corresponding bits in an orthogonalized FTN receiver

In (67), each h_i corresponds to the correlation between the *i*th transmitted pulse and the filter impulse response at the receiver and is expressed in (68).

$$h_i = \int_{-\infty}^{\infty} p(\tau - \frac{i-1}{k}T)\phi(t+\tau)d\tau|_{t=T/k} \tag{68}$$

This means that the channel matrix for the orthogonalized FTN MIMO system shown in Figure 30 can be expressed in (69) using the same $\mathbf{H}_{MIMO}$ defined in Chapter 2.

$$\mathbf{H}_{FTN_{OS}-MIMO} = \mathbf{H}_{FTN_{OS}} \otimes \mathbf{H}_{MIMO} \tag{69}$$

Also of interest is the noise covariance matrix $\mathbf{Q_z}$ described in (70). Because the noise samples are no longer correlated, the noise covariance matrix is an identity matrix of size *kN+k-1* by *kN+k-1* scaled by the noise variance σ^2.

$$\mathbf{Q}_z = \sigma^2 \mathbf{I}_{kN+k-1} \tag{70}$$

3.4. Ergodic Capacity of the Orthogonalized FTN MIMO Receiver

The capacity equation derived in Section 3.2 can still be used to calculate the capacity of the orthogonalized FTN MIMO receiver. It can also be noted that because the noise is now uncorrelated, the denominator in the expression takes the form of an identity matrix scaled by the noise variance. Thus the expression for a MIMO system with $\mathbf{H}_{\text{FTNMIMO}}$ substituted for $\mathbf{H}_{\text{MIMO}}$ can also be used.

Figure 32 shows the capacity of an orthogonalized FTN MIMO receiver compared to the traditional FTN MIMO receiver for a 2x2 MIMO system with varying FTN rates. Just as with the traditional receiver, increasing the FTN rate leads to an increase in capacity, particularly at higher SNRs. It is also interesting that the orthogonalized receiver has a capacity nearly identical to that of the traditional receiver. A possible explanation is that every kth sample at the orthogonalized receiver corresponds to the same sample that would be seen at one of the Nyquist rate sampling devices in the traditional receiver. For example, samples $0,k,2k,3k\ldots$ in the orthogonalized receiver would correspond to the samples on the first Nyquist rate stream in the traditional receiver, while samples $1,k+1,2k+1,3k+1\ldots$ in the orthogonalized receiver correspond to those of the second Nyquist rate stream in the traditional receiver. This means that the orthogonalized receiver obtains the same information as the traditional receiver, just relegated to a single stream.

Figure 33 shows the capacity of a 2xFTN system with the traditional receiver and the orthogonalized receiver for varying symmetric MIMO configurations. Once again, the performance of the traditional receiver and the orthogonalized receiver are almost identical.

The explanation above still holds true in this case: the orthogonalized receiver will gather the same information that the traditional receiver does; it is just in a different format.

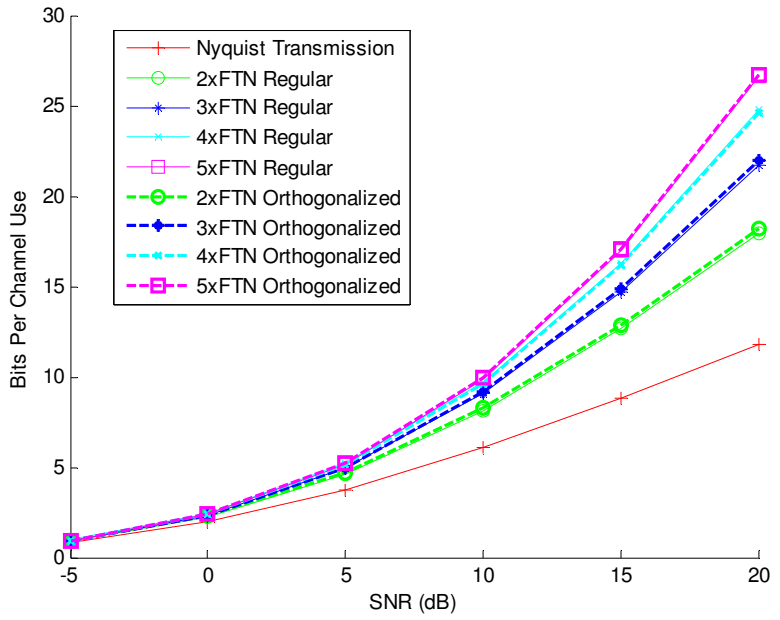

Figure 32. Comparison of traditional and orthogonalized FTN receivers in a 2x2 MIMO system

Figure 34 shows the capacity of an orthogonalized FTN MIMO receiver compared to the traditional FTN MIMO receiver for a 1x2 MIMO system with varying FTN rates. Just as with the traditional receiver, an increasing the FTN rate leads to an increase in capacity, particularly at higher SNRs. It is also interesting that the orthogonalized receiver has a nearly identical capacity to that of the traditional receiver even for more transmitting antennas than receiving antennas. This further indicates that both receivers, although using different architectures, are able to obtain the same capacity gains from the same transmitted FTN signal.

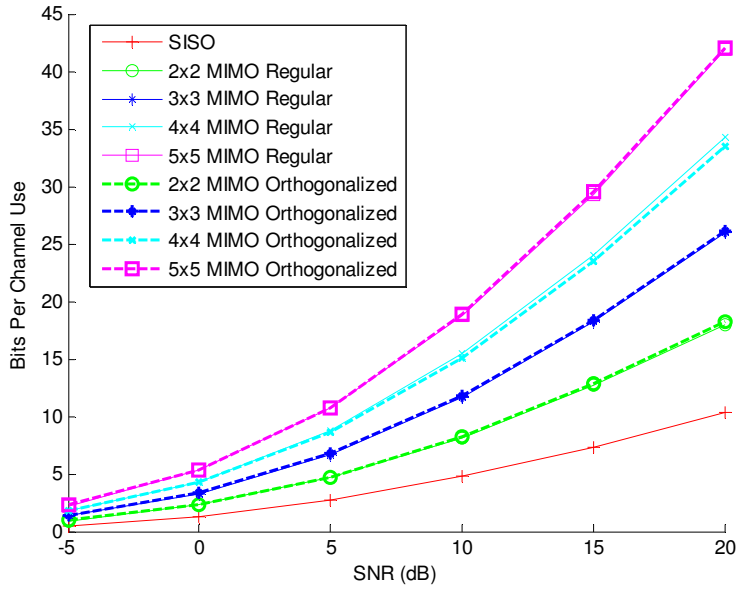

Figure 33. Comparison of traditional and orthogonalized receivers in a 2xFTN system with varying MIMO configurations

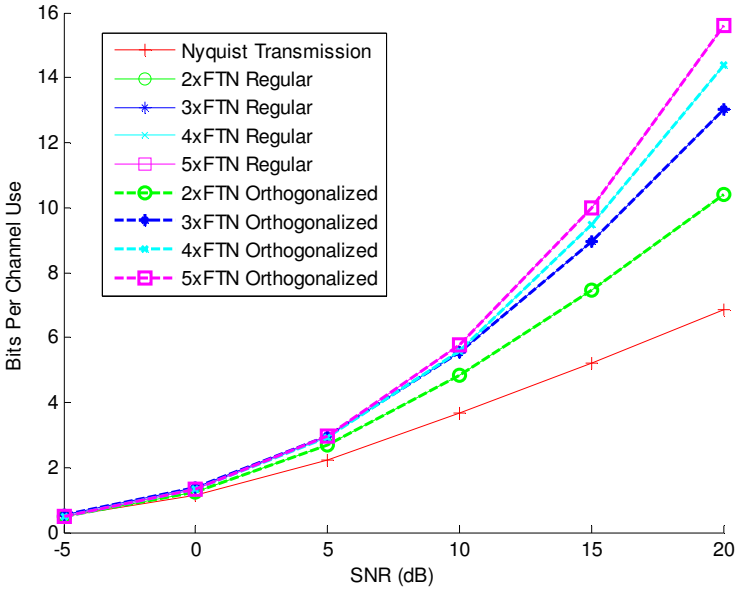

Figure 34. Capacity comparison of traditional and orthogonalized FTN receivers in a 2x1 MIMO system

Figure 35 shows the capacity of a 2xFTN system with the traditional receiver and the orthogonalized receiver for varying asymmetric MIMO configurations with more transmitters than receivers. Once again there is a high degree of similarity between the performance of the traditional receiver and the orthogonalized receiver. In general there is little gain from increasing the number of transmitting antennas without also increasing the number of FTN streams.

Figure 36 compares the orthogonalized receiver and the traditional receiver for 1x2 MIMO systems with varying FTN rates. Once again the orthogonalized receiver architecture and the traditional receiver architecture perform nearly identically in terms of capacity. This is likely due to the reasons stated previously.

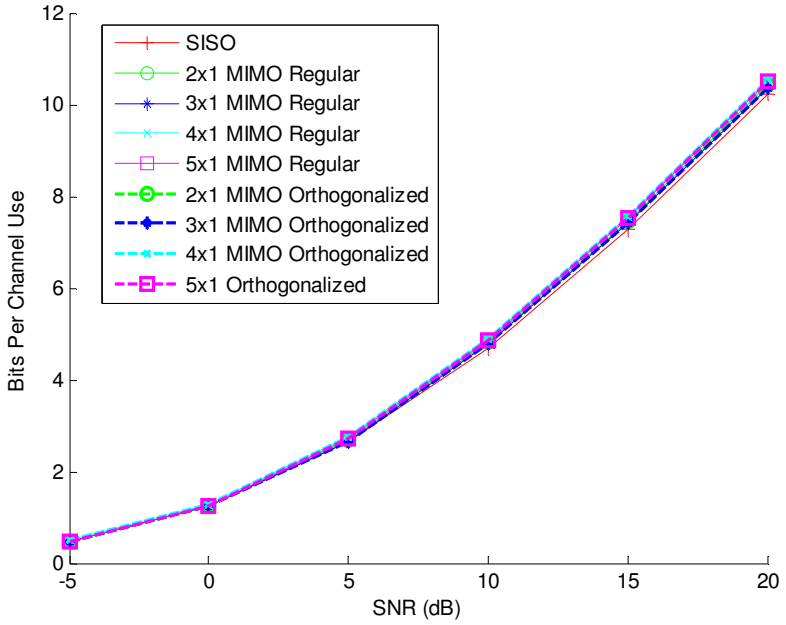

Figure 35. Comparison of traditional and orthogonalized FTN receivers with k=2 and various MISO configurations

Figure 37 compares the capacity of an orthogonalized FTN receiver and a traditional FTN receiver combined with various SIMO systems. Once again the two architectures perform nearly identically in terms of capacity.

Figure 38 compares the capacity of a SISO Nyquist rate system, a 2x2 MIMO system with no FTN, a 2xFTN SISO system with the orthogonalized receiver, a 2xFTN SISO system with the traditional receiver, and 2x2 MIMO systems with 2xFTN for both the orthogonalized and traditional receiver architectures. As before, the best case is the FTN and MIMO combined. In terms of capacity, the orthogonalized receiver performs nearly identically with the traditional architecture.

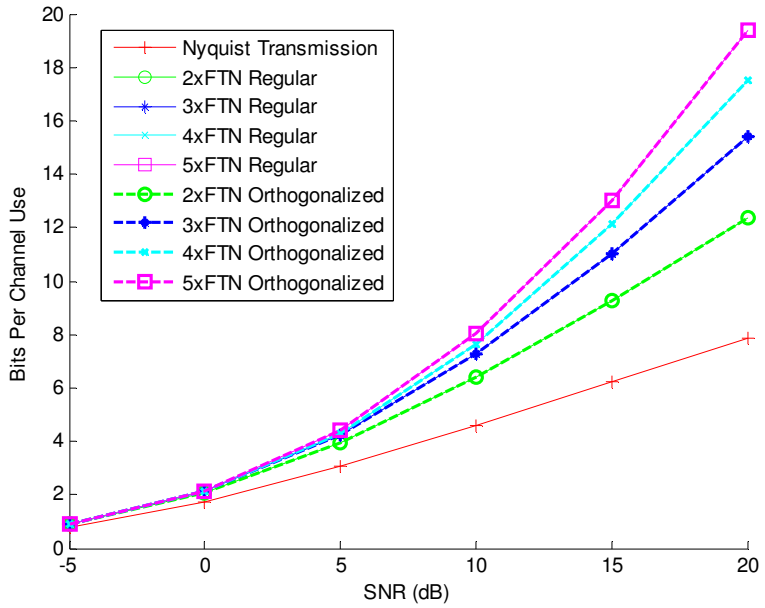

Figure 36. Capacity comparison of traditional and orthogonalized FTN receivers in a 1x2 SIMO system

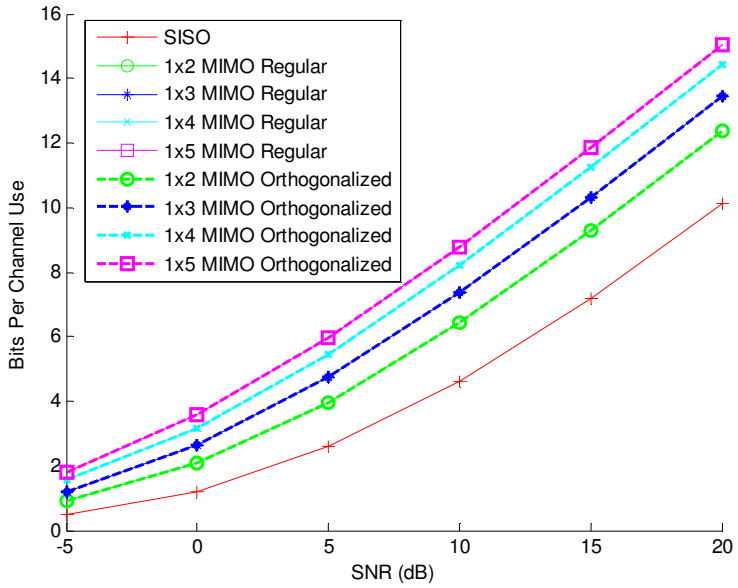

Figure 37. Capacity comparison of a 2xFTN system with traditional and orthoganalized receivers and varying SIMO configurations

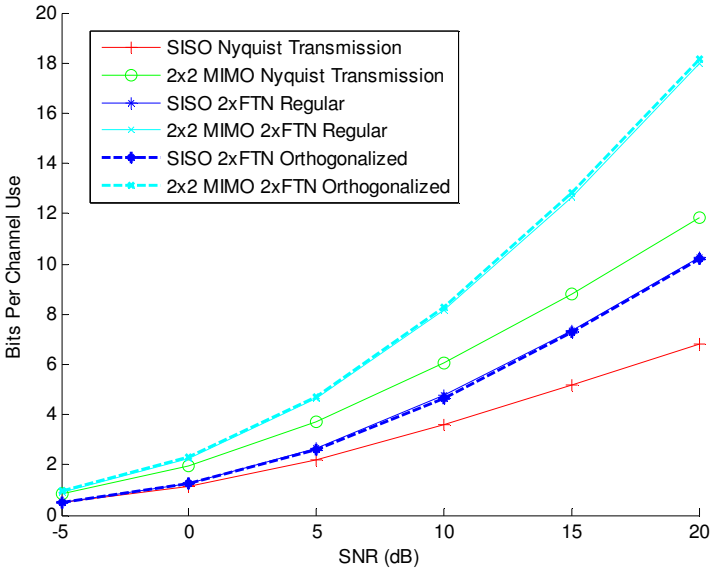

Figure 38. Comparison of various MIMO and FTN systems with traditional and orthogonalized FTN receiver architectures

Figure 39 compares the capacity of a SISO Nyquist rate system, a 2x1 MISO system with no FTN, a 2xFTN SISO system with the orthogonalized receiver, a 2xFTN SISO system with the traditional receiver, and 2x1 MISO systems with 2xFTN for both the orthogonalized and traditional receiver architectures. As before, the best case is the FTN and MISO combined with little extra capacity gain from the addition of MISO. In terms of capacity, the orthogonalized receiver performs nearly identically with the traditional architecture.

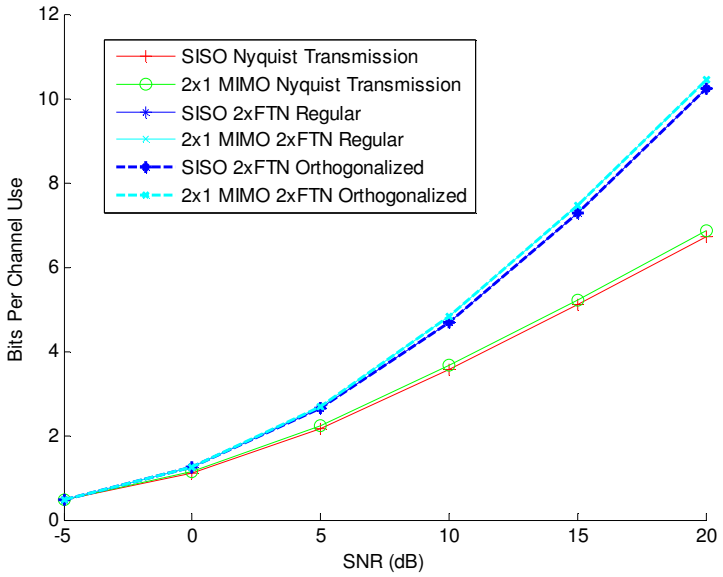

Figure 39. Capacities of various FTN and MISO systems with traditional and orthogonalized FTN receiver architectures

Figure 40 compares the capacity of a SISO Nyquist rate system, a 1x2 SIMO system with no FTN, a 2xFTN SISO system with the orthogonalized receiver, a 2xFTN SISO system with the traditional receiver, and 1x2 SIMO systems with 2xFTN for both the orthogonalized and traditional receiver architectures. As before, the best case is the FTN

and SIMO combined. In terms of capacity, the orthogonalized receiver performs nearly identically with the traditional architecture.

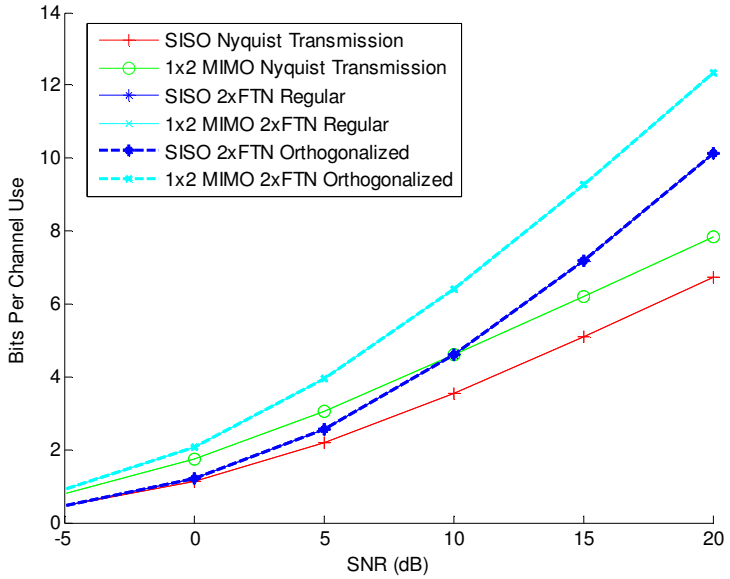

Figure 40. Capacities of various FTN and SIMO systems with traditional and orthogonalized FTN receiver architectures

In the previous results we have seen that the orthogonalized and traditional receivers perform nearly identically in terms of capacity for many varying system types. Because the complexity of the orthogonalized receiver is only increased with the number of receiving antennas, and not the product of receiving antennas and FTN streams as in the traditional receiver, the orthogonalized receiver provides a better value for information rate versus capacity. However, due to constraints such as only being able to use a rectangular pulse, and the high speed of the sampling device, this receiver may not be appropriate for all designs.

3.5. Undersampled FTN MIMO Receiver Architecture

In the previous two sections, a receiver with a single sampling device was used to de-correlate the noise in the received samples and alleviate this problem that occurred with the basic FTN architecture. However, the disadvantage of this architecture is that only a rectangular pulse can be used during transmission. Although this is applicable in industrial applications such as the OFDMA used in 4G, there are many cases where a system may need to be designed to function with additional pulse shapes. Furthermore, the sampling device was required to operate at k times the pulse rate. Even though the signal transmitted across the channel could be bandlimited, the receiving hardware may increase in cost or be impossible to realize for certain high-rate systems. In this section another receiver architecture with uncorrelated noise is proposed. This system uses the same receiver structure as a Nyquist rate system and relies on a decoder to attempt to reconstruct the transmitted packet with $N+1$ samples gathered at each antenna at the receiver. Because there are now fewer samples than transmitted symbols, this architecture is called the undersampled FTN architecture.

Figure 41 shows an example of an undersampled FTN MIMO system. This system uses the same transmitter architecture as the basic FTN MIMO system described in Section 3.1 so the transmitted signal at the jth antenna $x_j(t)$ is still expressed by (44). Furthermore, AWGN is still assumed to be added independently at each antenna which means the received signal on the ith antenna $r_i(t)$ can still be expressed by (45). Each received signal $r_i(t)$ is passed through a filter matched to the transmitted pulse shape. The matched filter has an impulse response $p^*(-t)$ so that it acts as a correlator with the transmitted pulse.

However, in this under-sampled system, rather than having k matched filters at each receive antenna, there is only one. This means the output of the matched filter on the ith receive antenna $y_i(t)$ can be described by (71).

$$y_i(t) = \int_{-\infty}^{\infty} r_i(\tau) p^*(\tau + t) d\tau \tag{71}$$

The waveform $y_i(t)$ is then sampled every T seconds just as in a Nyquist rate system. The discrete time waveform $y_i[n]$ can therefore be described by (72).

$$y_i[n] = y_i(t)\big|_{t=nT} \tag{72}$$

Just as in the orthogonalized FTN MIMO system, each sample no longer corresponds to a single transmitted symbol, but rather to multiple symbols that occupy the same time instant. As a result, it is necessary to use a soft decision decoder to reconstruct the transmitted packet from the channel outputs.

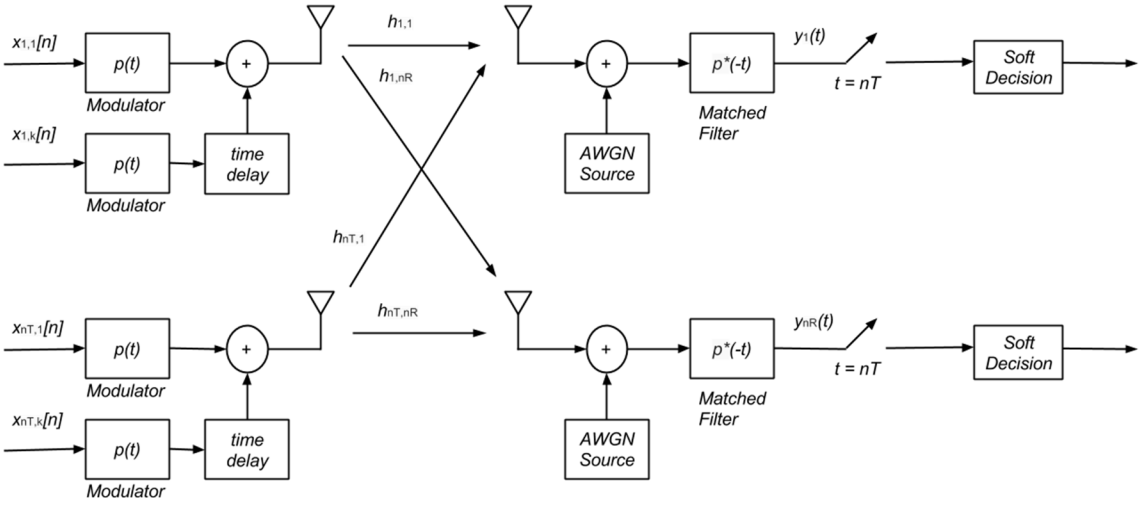

Figure 41. Block diagram of an undersampled FTN MIMO System

The relationship between the output and input to this system can also be described by the vector equation **y=Hx+z**. In this case, the input vector **x** remains the same as in the FTN MIMO system described in Section 3.1 because the same transmitter structure is used. Now however, the output vector **y** will be defined by (73). Note that there are now only *N*+1 samples gathered per packet per antenna.

$$\mathbf{y} = \left(y_1[1]\ y_1[2]\ y_1[3] \cdots y_1[N+1]\ y_2[1]\ y_2[2] \cdots y_{n_T}[N+1] \right)^T \tag{73}$$

However, because there is only one sample and hold device per antenna, the noise on the received samples in uncorrelated. The noise vector **z** is defined in (74) where $z_{i,j}$ corresponds to the noise on the *j*th sample at the *i*th receiving antenna. All entries of **z** are assumed to be zero mean Gaussian random variables with variance σ^2.

$$\mathbf{z} = \left(z_{1,1}\ z_{1,2}\ z_{1,3} \cdots z_{1,N+1}\ z_{2,1}\ z_{2,2} \cdots z_{n_T,N+1} \right)^T \tag{74}$$

The channel matrix **H** can still be described as the kronecker product of the MIMO channel matrix and the FTN channel matrix. However, this system has a different FTN channel matrix due to the unconventional FTN receiver architecture. In general, a channel matrix **H** can be written such that each entry $h_{i,j}$ denotes the correlation between the *i*th transmitted symbol and the *j*th received sample. In this receiver, each received sample corresponds to pulses on the first FTN stream. This means that the correlation between a received sample and its corresponding pulse in the first FTN stream is always one. Each sample also has partial correlation with *2k* bits on the additional FTN streams. Note that *kN* symbols were transmitted, but only *N+1* samples are received causing the channel matrix to be of size *kN* by *N+1*. Figure 42 helps to visualize the new sampling scheme by

showing the sample times for a 2xFTN system with this receiver architecture. In this figure the black rectangles refer to transmitted pulses. The number contained within each rectangle shows the column to which that pulse corresponds in the channel matrix. The red lines represent the sampling times at the receiver. Equation (75) demonstrates the new form of the FTN channel matrix.

$$\mathbf{H}_{FTN_{US}} = \begin{pmatrix} 1 & h_{-1} & \cdots & h_{-k} & h_{-(k+1)} & h_{-(k+2)} & \cdots & \cdots & \cdots & \cdots & h_{-(kN-1)} \\ h_{k+1} & h_k & \cdots & h_1 & 1 & h_{-1} & \cdots & h_{-k} & \cdots & \cdots & h_{-(kN-2)} \\ \vdots & \ddots & \ddots & \ddots & \ddots & \ddots & \ddots & \ddots & \ddots & \ddots & \vdots \\ h_{kN-1} & \cdots & \cdots & \cdots & \cdots & \cdots & \cdots & \cdots & \cdots & h_1 & 1 \end{pmatrix} \quad (75)$$

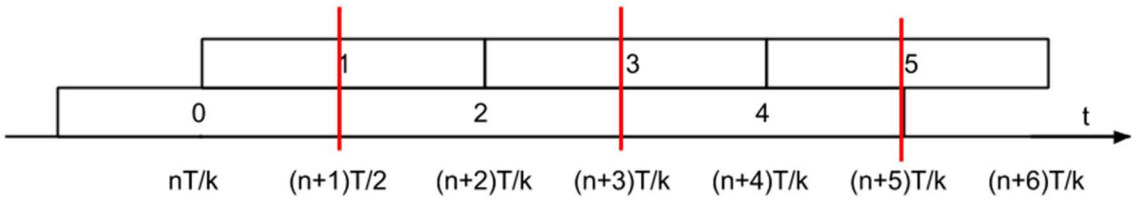

Figure 42. Sample times and their corresponding bits in an undersampled FTN receiver

The channel matrix entries h_i are defined in equation (76). It may help to think of the channel matrix as being similar to MIMO in the case where there are more transmitters than receivers since the channel has more inputs than outputs.

$$h_i = \int_{-\infty}^{\infty} p(\tau - i\frac{T}{k}) p^*(t-\tau) d\tau |_{t=T} \quad (76)$$

Using the undersampled FTN channel matrix defined in (75), the channel matrix for the undersampled FTN MIMO system shown in Figure 41 can be expressed in (77) using the same $\mathbf{H}_{MIMO}$ defined in Chapter 2.

$$\mathbf{H}_{FTN_{US}-MIMO} = \mathbf{H}_{FTN_{US}} \otimes \mathbf{H}_{MIMO} \quad (77)$$

Also of interest is the noise covariance matrix $\mathbf{Q_z}$ which is described in (78). The noise in each sample is uncorrelated because there is only one matched filter and sampling device per antenna. Therefore, the noise covariance matrix is described as an identity matrix of size *N+1* by *N+1* scaled by the noise variance σ^2.

$$\mathbf{Q}_z = \sigma^2 \mathbf{I}_{N+1} \tag{78}$$

In the case where channel state information is known only at the transmitter, the transmitter's best option is to send bits independently of one another. This means that the data covariance matrix $\mathbf{Q_x}$ is an identity matrix with dimensions *Nk* by *Nk*.

3.6. Ergodic Capacity of the Undersampled FTN MIMO Receiver

The capacity equation derived in Section 3.2 is still valid to calculate the capacity of the undersampled FTN MIMO receiver. It can also be noted that because the noise is now uncorrelated, the denominator in the expression takes the form of an identity matrix scaled by the noise variance. Thus the expression for the capacity of a MIMO system from (60) with $\mathbf{H}_{FTNMIMO}$ substituted for $\mathbf{H}_{MIMO}$ can also be used.

Figure 43 shows the capacity of an undersampled FTN MIMO receiver compared to the traditional FTN MIMO receiver for a 2x2 MIMO system with varying FTN rates. Unlike the traditional and orthogonalized receiver, the undersampled FTN receiver architecture does not appear to lead to an increase in capacity as more FTN streams are added. Furthermore, it performs slightly worse than the traditional receiver. This slightly worse performance is likely due to the fact that there is now self-interference between

transmitted FTN streams. Even though the receiver knows the structure of the channel matrix, the transmitter is forced to allocate power equally to all FTN streams in the CSIR case. This means that adding more streams only increases self-interference without any way to fully compensate for it at the receiver.

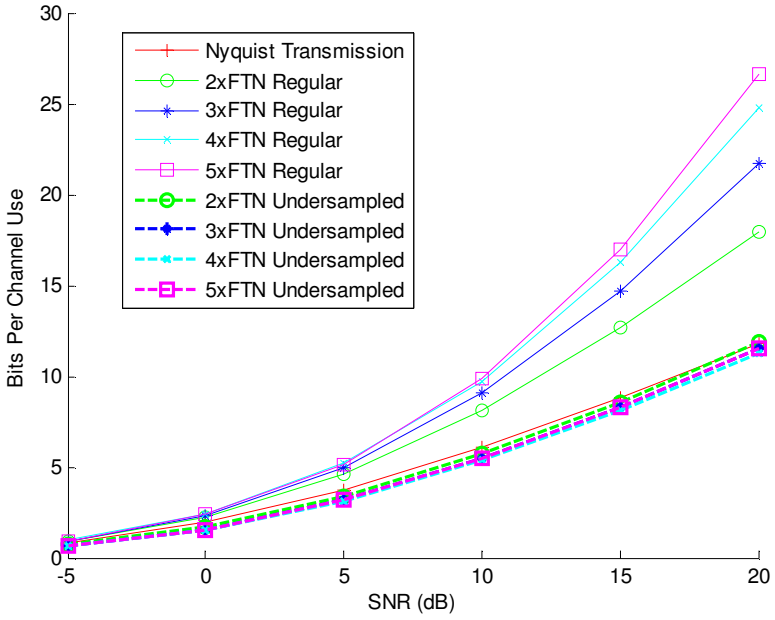

Figure 43. Capacity comparison of a 2x2 MIMO System with varying FTN rates and a traditional and undersampled FTN receiver architecture

Figure 44 shows the capacity of an undersampled FTN MIMO receiver compared to the traditional FTN MIMO receiver for a 2xFTN system with varying symmetric MIMO configurations. The MIMO gain appears to boost the capacity of the undersampled system above that of the Nyquist rate SISO system, however, the traditional receiver architecture performs better.

Figure 45 shows the capacity of an undersampled FTN MIMO receiver compared to the traditional FTN MIMO receiver for a 2x1 MISO system with varying FTN rates. Unlike the traditional and orthogonalized receiver, the undersampled FTN receiver architecture does not appear to lead to an increase in capacity as more FTN streams are added.

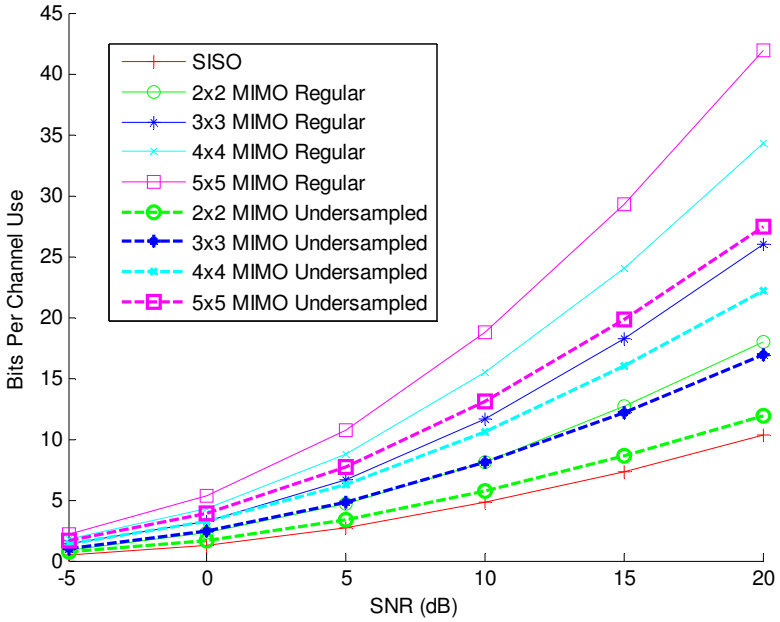

Figure 44. Capacity comparison a 2xFTN system with various MIMO configurations for traditional and undersampled FTN receiver architectures

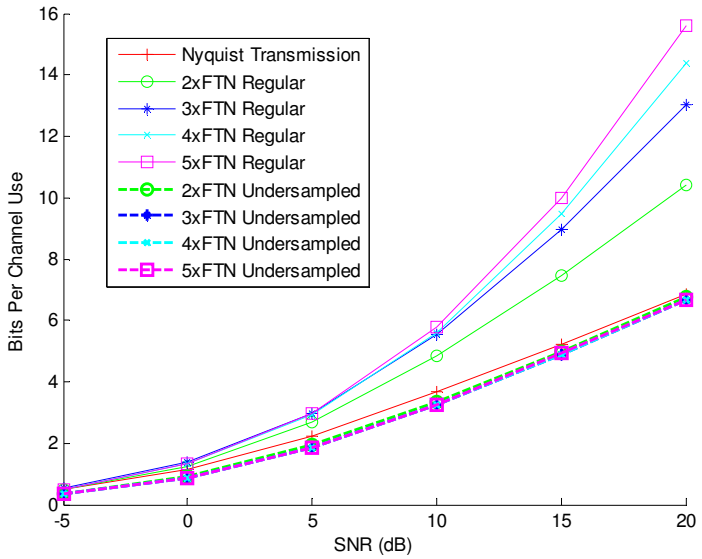

Figure 45. Capacity comparison of a 2x1 MISO system with FTN rate *k*=1…5 for traditional and undersampled FTN receiver architectures

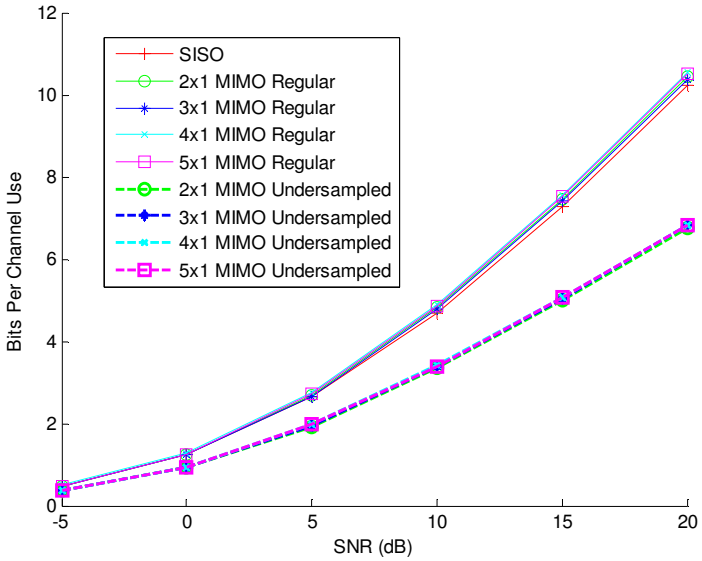

Figure 46. Capacity comparison of a 2xFTN system with various MISO configurations for traditional and undersampled FTN receiver architectures

Figure 46 shows the capacity of an undersampled FTN MIMO receiver compared to the traditional FTN MIMO receiver for a 2xFTN system with varying MISO system configurations. The undersampled system performs worse than the regularly sampled system in all cases.

Figure 47 shows the capacity of an undersampled FTN MIMO receiver compared to the traditional FTN MIMO receiver for a 1x2 SIMO system with varying FTN rates. Unlike the traditional and orthogonalized receiver, the undersampled FTN receiver architecture does not appear to lead to an increase in capacity as more FTN streams are added.

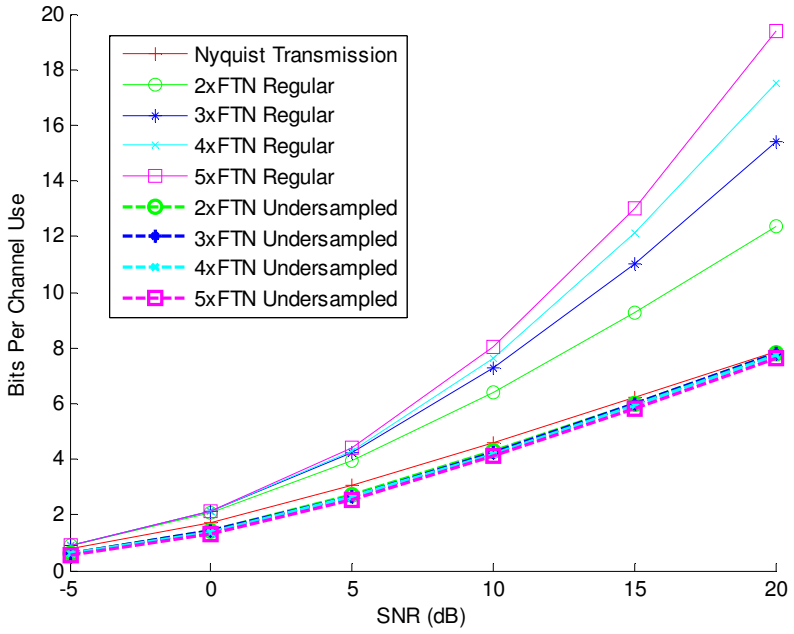

Figure 47. Capacity comparison of a 1x2 SIMO system with various FTN rates for traditional and undersampled FTN receiver architectures

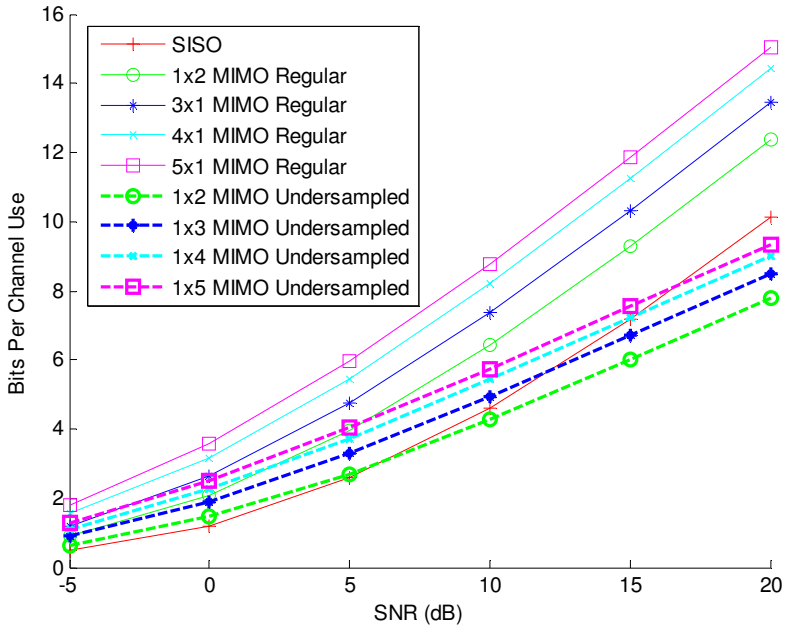

Figure 48. Capacity comparison of a 2xFTN system with various SIMO configurations for traditional and undersampled FTN receiver architectures

Figure 48 shows the capacity of an undersampled FTN MIMO receiver compared to the traditional FTN MIMO receiver for a 2xFTN system with varying SIMO system configurations. The undersampled SIMO systems perform better than the traditional 2xFTN SISO system for lower SNRs, but lose the advantage at higher SNRs. Furthermore, the undersampled SIMO systems perform worse than their traditional counterparts.

Figure 49 shows the capacity of an undersampled FTN MIMO receiver compared to the traditional FTN MIMO receiver for varying FTN rates and varying SIMO system configurations. The undersampled receiver appears to perform worse than the Nyquist rate system in all cases.

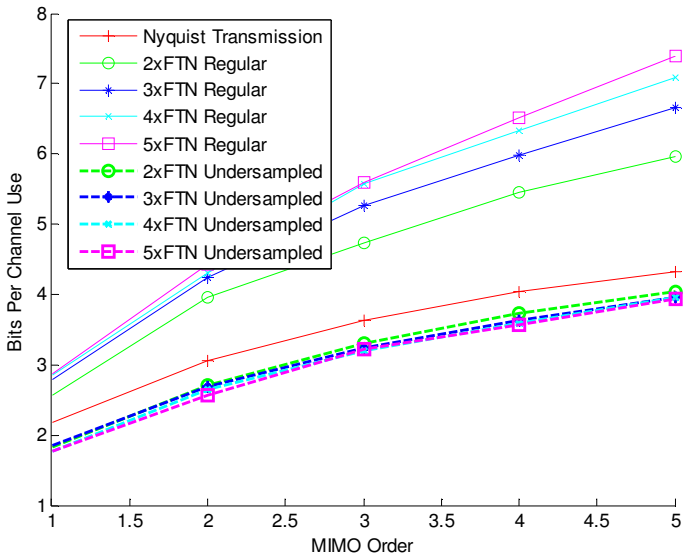

Figure 49. Capacity comparison of varying FTN rates and SIMO configurations for traditional and undersampled FTN receiver architectures

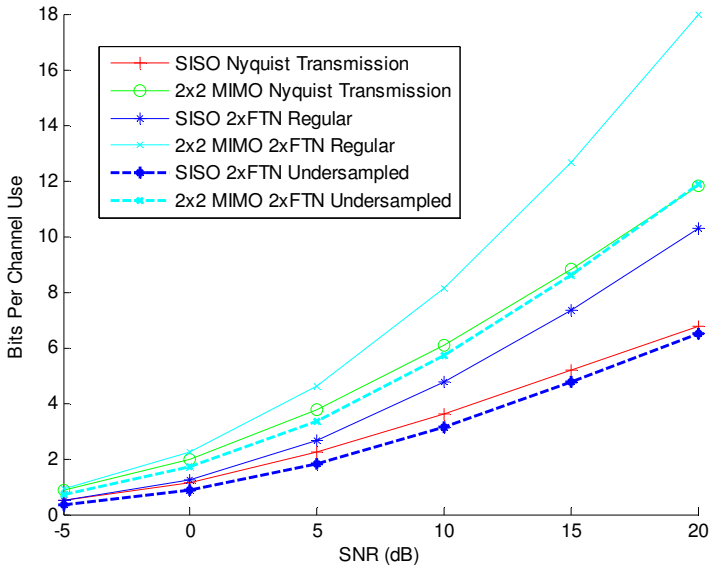

Figure 50. Capacity comparison of SISO and MIMO Nyquist rate systems with various MIMO and SISO FTN systems with traditional and undersampled receivers

Figure 50 compares the capacities of a SISO Nyquist rate system, a 2x2 MIMO Nyquist rate system, a SISO 2xFTN system with a traditional receiver, a 2x2 MIMO 2xFTN system with a traditional receiver, a SISO 2xFTN system with an undersampled receiver, and a 2x2 MIMO 2xFTN system with an undersampled receiver. From this graph it appears that the undersampled receiver architectures perform worse than the corresponding traditional receiver architectures across the analyzed range of SNRs.

Figure 51 compares the capacities of a SISO Nyquist rate system, a 2x1 MISO Nyquist rate system, a SISO 2xFTN system with a traditional receiver, a 2x1 MISO 2xFTN system with a traditional receiver, a SISO 2xFTN system with an undersampled receiver, and a 2x1 MISO 2xFTN system with an undersampled receiver. From this graph it appears that the undersampled receiver architectures perform worse than the corresponding traditional receiver architectures across the analyzed range of SNRs.

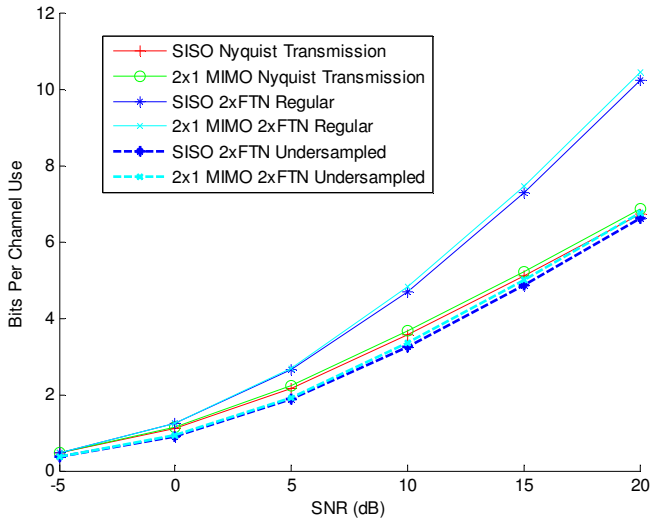

Figure 51. Capacity comparison of SISO and MISO Nyquist rate systems with various MISO and SISO FTN systems with traditional and undersampled receivers

Figure 52 compares the capacities of a SISO Nyquist rate system, a 1x2 SIMO Nyquist rate system, a SISO 2xFTN system with a traditional receiver, a 1x2 SIMO 2xFTN system with a traditional receiver, a SISO 2xFTN system with an undersampled receiver, and a 1x2 SIMO 2xFTN system with an undersampled receiver. From this graph it appears that the undersampled receiver architectures perform worse than the corresponding traditional receiver architectures across the analyzed range of SNRs.

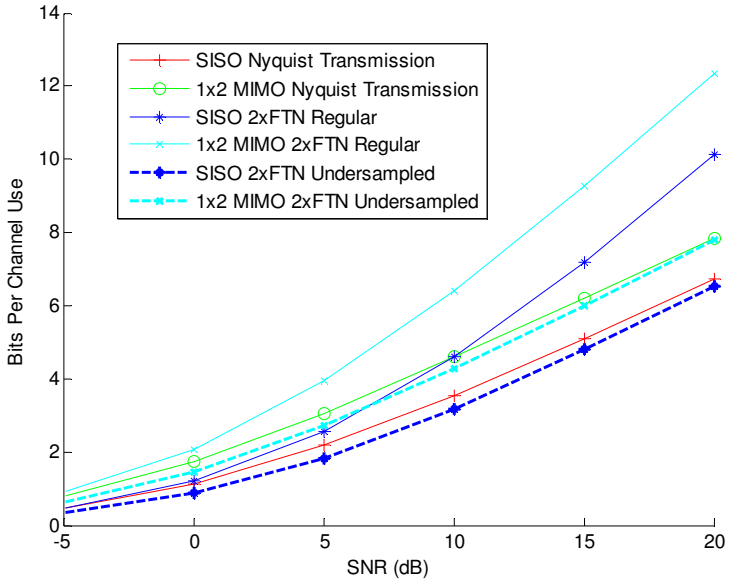

Figure 52. Capacity comparison of a SISO and SIMO Nyquist rate systems with various SIMO and SISO FTN systems with traditional and undersampled architectures

3.7. FTN MIMO and CSIT

In the orthogonalized FTN receiver proposed in Section 3.3, the noise on the received samples is no longer correlated. This means that the capacity of the system can now be calculated using the same capacity equation as a MIMO system described in (22). This also means that the channel matrix can be decomposed into singular values that represent the gains of parallel Gaussian channels. Furthermore, just as in the MIMO case, if the transmitter knows the condition of the channel before transmitting – the transmitter knows the channel matrix $\mathbf{H}_{\text{FTN-MIMO-OS}}$ or $\mathbf{H}_{\text{FTN-MIMO-US}}$ – then the transmitted symbols can be precoded to take advantage of the channel conditions. In this case, the optimal solution is still to allocate the most power to channels with high gains and the least power to channels with low gains. This solution can be found by water filling. The results below show the capacities of various orthogonalized FTN systems with water filling and CSIT compared to the traditional receiver with CSIR only.

Figure 53 shows the capacity of a 2x2 MIMO system combined with an orthogonalized FTN receiver with CSIT and a traditional FTN receiver with CSIR. It can be observed the CSIT leads to an increased capacity at low SNRs, with diminishing gains compared to the CSIR case at high SNRs. This is similar to CSIT in a pure MIMO system where the precoding gains are pronounced at low SNRs and negligible at higher SNRs.

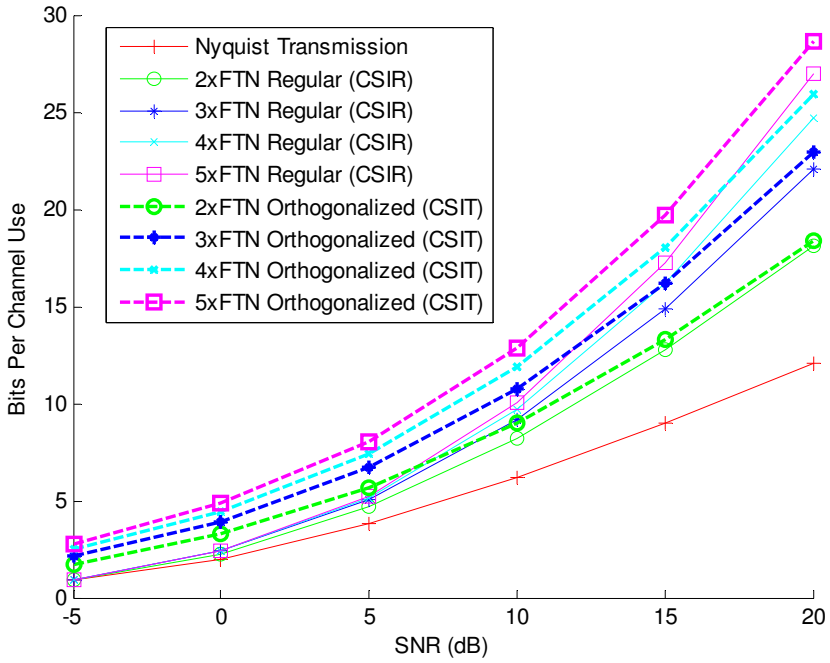

Figure 53. Capacity comparison of a 2x2 MIMO system with various FTN rates for traditional receiver architecture with CSIR and orthogonalized receiver architecture with CSIT

Figure 54 shows the capacities for a 2xFTN system with an orthogonalized receiver and CSIT and a 2xFTN system with a traditional receiver and CSIR for various symmetric MIMO configurations. In this case the system with CSIT outperforms CSIR system at lower SNRS, but approaches the same capacity at higher ones. At lower SNRs precoding helps the transmitter take advantage of high quality parallel Gaussian channels, but at higher SNRs, more high quality channels exist so the gain is not as pronounced.

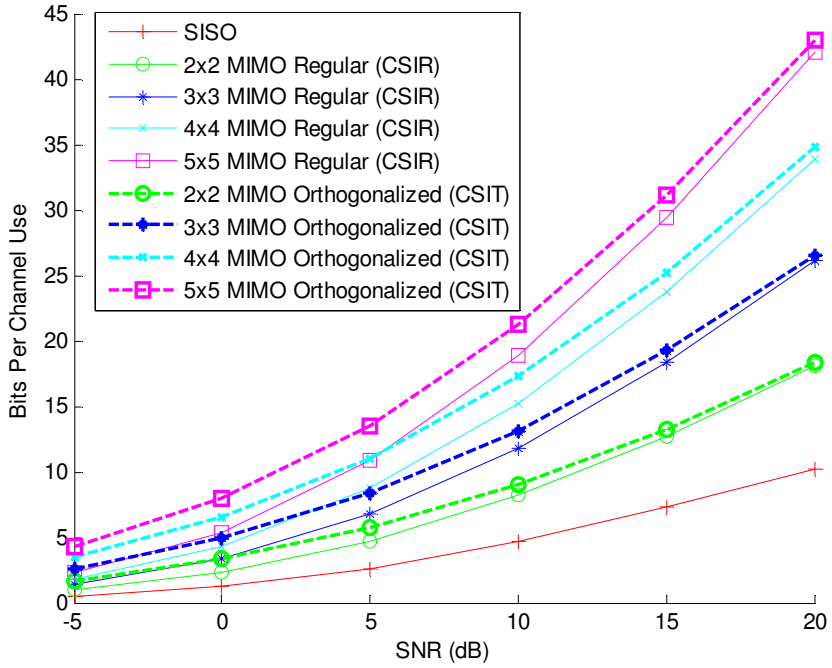

Figure 54. Capacity comparison of a 2xFTN system with various MMO configurations for traditional receiver architecture with CSIR and orthogonalized receiver architecture with CSIT

Figure 55 shows the capacities for various FTN MIMO systems with a traditional receiver and CSIR or an orthogonalized receiver with CSIT when the SNR is 5dB. It compares systems from Nyquist rate to 5xFTN and SISO to 5x5 MIMO. This graph shows that the precoding gain is so great at an SNR of 5dB that a 2xFTN system with CSIT will outperform a 5xFTN system with the same number of antennas and CSIR only. It can be observed that both increasing MIMO order and increasing the FTN rate lead to capacity increased capacity gains over a system's CSIR counterpart. As the quality of CSI degrades, it is also presumable that the channel capacity would degrade as well, but the exact relationship is outside of the scope of this thesis and could serve as an area for future research.

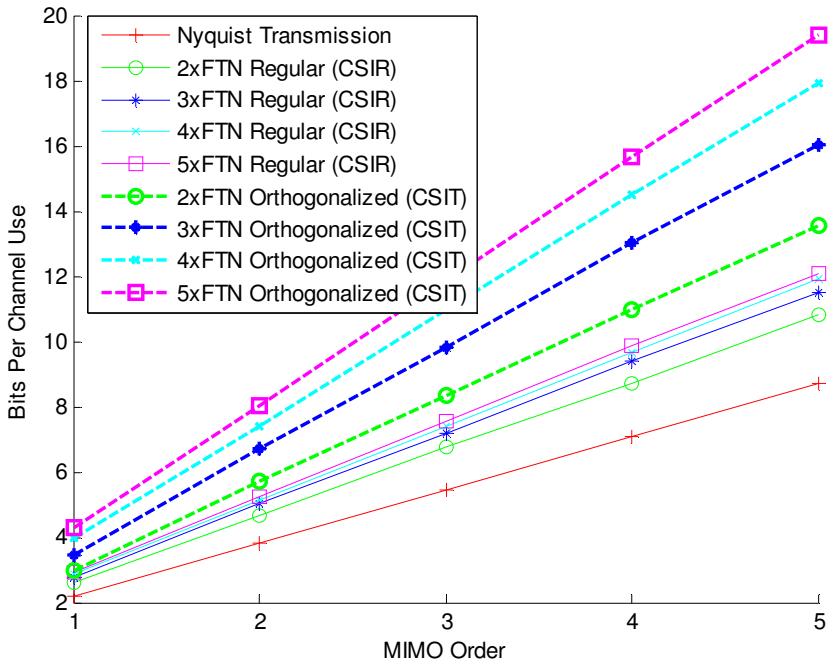

Figure 55. Capacity comparison of a various MIMO and FTN systems with traditional receiver architecture with CSIR and orthogonalized architecture with CSIT at SNR=5dB

Figure 56 shows the capacity of a 2x1 MISO system combined with an orthogonalized FTN receiver with CSIT and a traditional FTN receiver with CSIR. It can be observed that in this case, CSIT also leads to a capacity increase at low SNRs with a diminished gain compared to the corresponding CSIR system at higher SNRs. One way of looking at this result of converging capacities at higher SNRs is that the number of degrees of freedom of corresponding traditional and orthogonalized systems is the same. This means that as the SNR improves and there are more good parallel channels, gain from precoding is no longer as pronounced and the dominant limiting factor of system capacity is from the dimensionality of the system.

Figure 57 shows the capacities for a 2xFTN system with an orthogonalized receiver and CSIT, and a 2xFTN system with a traditional receiver and CSIR for various MISO configurations. It can be observed that the orthogonalized system with CSIT performs better than the traditional system with CSIR. This figure is interesting because it shows that there is a capacity gain introduced by CSIT, but the gain does not increase noticeably as more transmitter antennas are added, but the receiver configuration stays the same. This parodies the capacity of a Nyquist rate MISO system where an increasing number of transmitting antennas without increasing the number of receiving antennas only leads to a negligible capacity gain. A way of understanding this is that, even by coding perfectly at the transmitter, the number of parallel Gaussian channels that can be generated by this system is still limited by the number of receiving antennas.

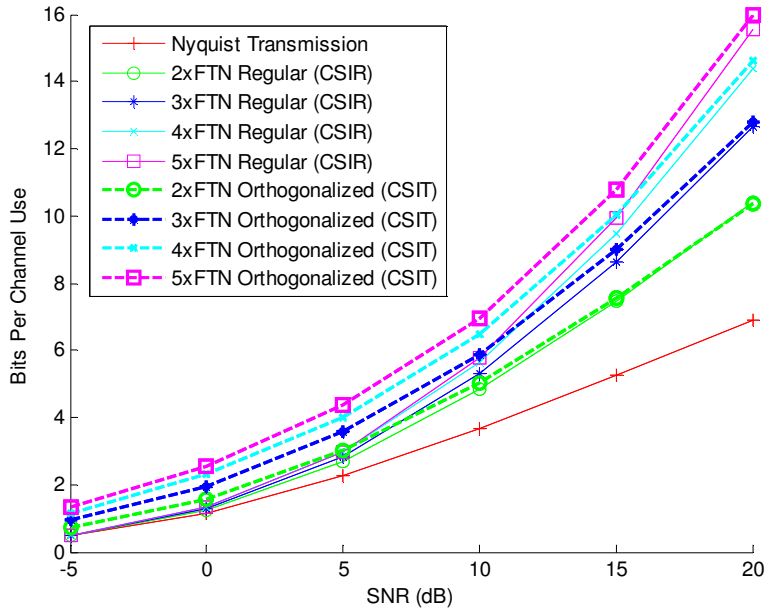

Figure 56. Capacity comparison of a 2x1 MISO system with various FTN rates for traditional receiver architecture with CSIR and orthogonalized receiver architecture with CSIT

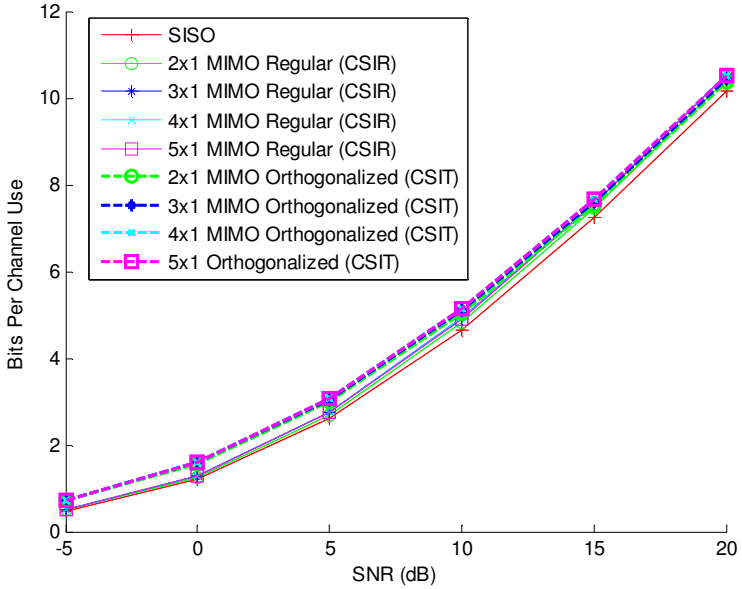

Figure 57. Capacity comparison of a 2xFTN system with various MISO configurations for traditional receiver architecture with CSIR and orthogonalized receiver architecture with CSIT

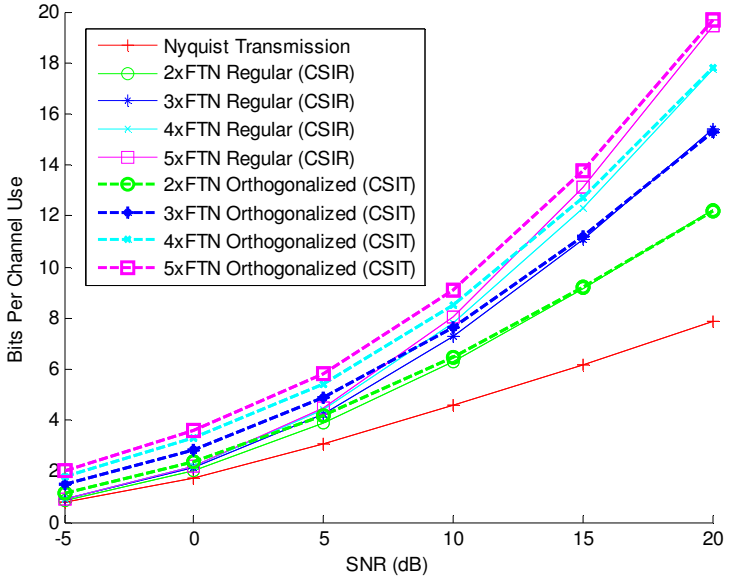

Figure 58. Capacity comparison of a 1x2 SIMO system with various FTN rates for traditional receiver architecture with CSIR and orthogonalized receiver architecture with CSIT

Figure 58 shows the capacity of a 1x2 SIMO system combined with an orthogonalized FTN receiver with CSIT and a traditional FTN receiver with CSIR. It can be observed that just as with the FTN MIMO systems described above, CSIT leads to a capacity increase at lower SNRs, but approaches the CSIR capacity as SNR increases. Once again, this is caused because precoding allows the transmitter to smartly allocate power when some of the Gaussian channels are poor (as in the low SNR case), but when there are numerous high quality channels it is no longer as important.

Figure 59 shows the capacities for a 2xFTN system with an orthogonalized receiver and CSIT and a 2xFTN system with a traditional receiver and CSIR for various SIMO configurations. Once again, the systems with CSIT outperform their corresponding CSIR systems at lower SNRs, but gain is diminished at higher SNRs. In this graph however, there is a clear increase in capacity caused by increasing the number of receiving antennas. Therefore, in this case, the gain from increasing the number of receiving antennas and thereby receiver diversity outstrips any precoding gains that occurred by introducing CSIT.

Figure 60 shows the capacities for various FTN SIMO systems with a traditional receiver and CSIR or an orthogonalized receiver with CSIT when the SNR is 5dB. Based on this figure, we can see that a system with CSIT will always outperform its corresponding CSIR system at this SNR. It can also be seen that in the SIMO case, although the gains from increasing number of antennas become less pronounced as more antennas are added, gains from CSIT do not appear to suffer from the same diminishing returns. Furthermore, it appears that the gains from CSIT are actually increased with higher FTN rate systems,

indicating that the precoding is not just taking advantage of parallel Gaussian channels generated by SIMO, but also those generated by FTN.

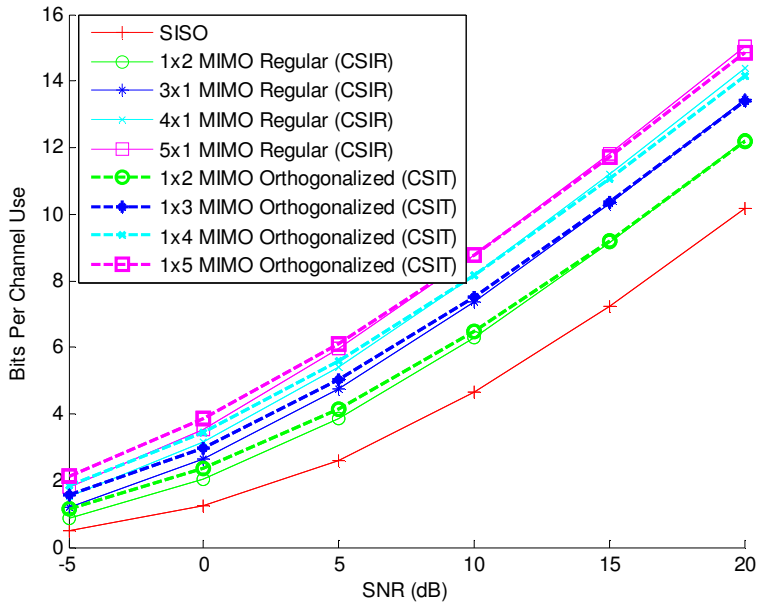

Figure 59. Capacity comparison of a 2xFTN system with various SIMO configurations for traditional receiver architecture with CSIR and orthogonalized receiver architecture with CSIT

Figure 61 compares a SISO system with Nyquist rate transmission, a 2x2 MIMO system with Nyquist Transmission, a SISO system with 2xFTN and a traditional receiver with CSIR only, a SISO system with 2xFTN and an orthogonalized receiver with CSIT, a 2x2 MIMO system with 2xFTN and a traditional receiver architecture, and a 2x2 MIMO system with 2xFTN and an orthogonalized receiver with CSIT. It can be observed that the systems with CSIT outperform their counterparts at lower SNRs, but converge on the same capacity as SNR increases. It can also be observed that the precoding gains are greater in

the system with MIMO and FTN than the system with FTN alone. This indicates that the precoding gains from MIMO play an important role in the final capacity of the CSIT system.

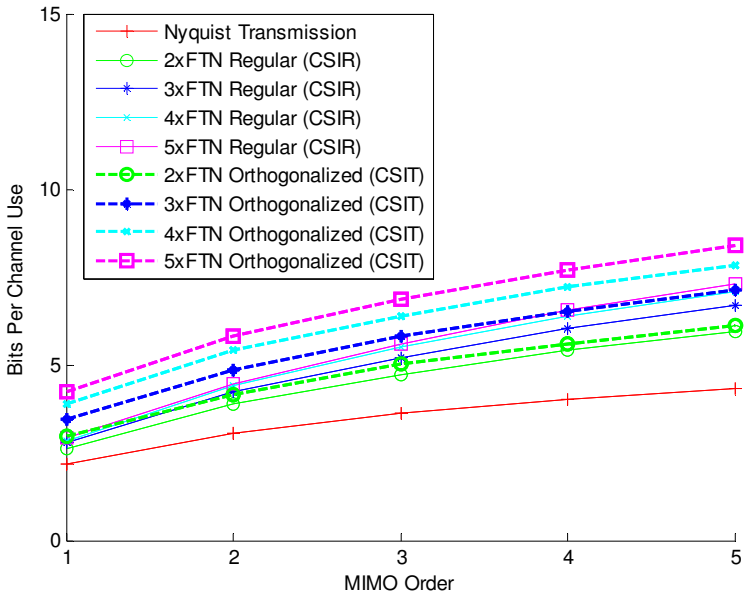

Figure 60. Capacity comparison of a various SIMO and FTN systems with traditional receiver architecture with CSIR and orthogonalized architecture with CSIT at SNR=5dB

Figure 62 compares a SISO system with Nyquist rate transmission, a 2x1 MISO system with Nyquist Transmission, a SISO system with 2xFTN and a traditional receiver with CSIR only, a SISO system with 2xFTN and an orthogonalized receiver with CSIT, a 2x1 MISO system with 2xFTN and a traditional receiver architecture, and a 2x1 MISO system with 2xFTN and an orthogonalized receiver with CSIT. In this case, both systems with CSIT have roughly the same performance despite one having double the number of transmitting antennas. However, both systems perform better than their CSIR counterparts. This is behavior is similar to what was observed previously in MISO systems.

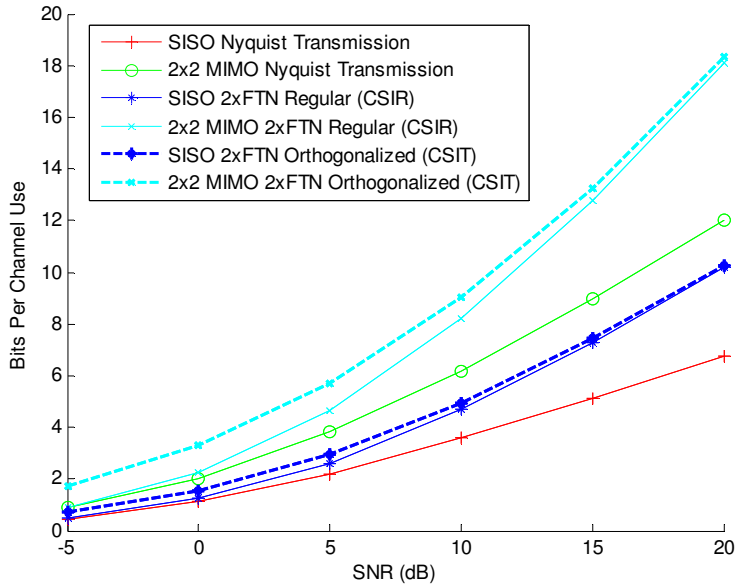

Figure 61. Capacity comparison of various MIMO and FTN systems with traditional receiver architecture with CSIR and orthogonalized receiver architecture with CSIT

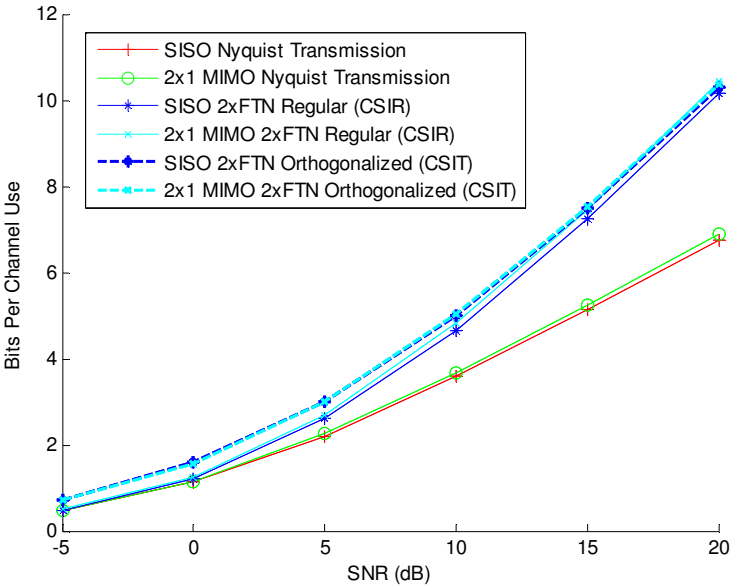

Figure 62. Capacity comparison of various MISO and FTN systems with traditional receiver architecture with CSIR and orthogonalized receiver architecture with CSIT

Figure 63 compares a SISO system with Nyquist rate transmission, a 1x2 SIMO system with Nyquist Transmission, a SISO system with 2xFTN and a traditional receiver with CSIR only, a SISO system with 2xFTN and an orthogonalized receiver with CSIT, a 1x2 SIMO system with 2xFTN and a traditional receiver architecture, and a 2x1 SIMO system with 2xFTN and an orthogonalized receiver with CSIT. It can be observed that the systems with CSIT outperform their CSIR counterparts at lower SNRs but converge to the same capacity at higher SNRs. This is consistent with the previously discussed results. It can also be observed that the gain from precoding does not seem to change much even when the number of receiving antennas is doubled, indicating that the precoding gain is influenced more by FTN rate in this case.

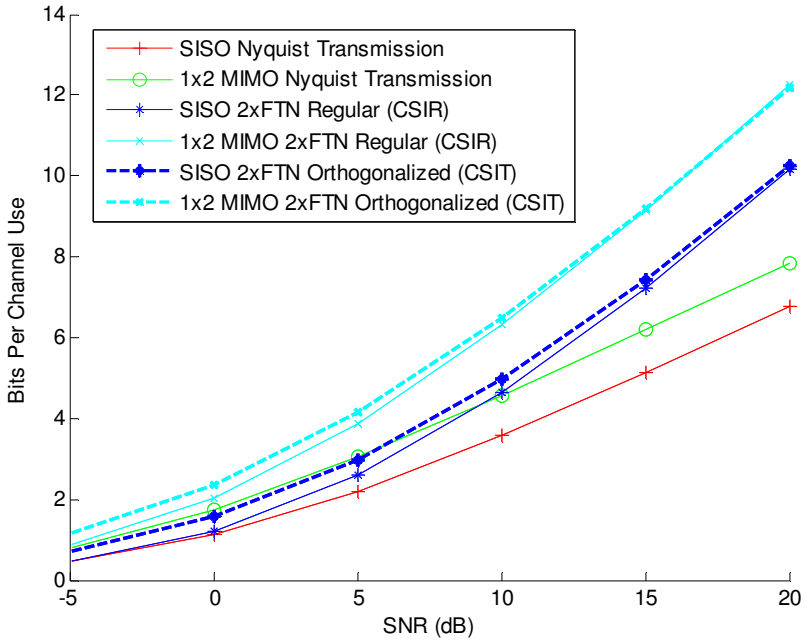

Figure 63. Capacity comparison of various SIMO and FTN systems with traditional receiver architecture with CSIR and orthogonalized receiver architecture with CSIT

Chapter 4. Conclusions and Future Research

Motivation

This research was motivated by the ever increasing requirement for mobile data communications. Currently, wireless subscribers have many different protocols from which to obtain mobile database. These include decentralized services like Wi-Fi and controlled networks such as LTE. The 5th generation of mobile networks intends to unify as many of these competing protocols as possible and provide more data to more subscribers than ever before. Furthermore, with the advent of sensor networks and the Internet of things, machine to machine protocols will require greater data transfer rates over a limited spectrum. Previous communications protocols have relied heavily on orthogonal communication systems; that is to say, every transmitted symbol or packet occupies its own resource block and the system attempts to mitigate interference between data. However, due to limited spectrum and power requirements, the next generation of mobile systems will likely have to use non-orthogonal communication systems to achieve the desired data rates. Initial results show that non-orthogonal communication systems have a potential for increased capacity compared to their traditional counterparts. This extra capacity comes at the expense of system complexity, though the continued improvement of microelectronics now have the potential to make these systems possible on mobile devices.

Research Contributions

This research focused on two types of non-orthogonal communication systems: MIMO and FTN. These two technologies are combined in a single system and the Shannon capacity of that system is observed. Because traditional FTN receivers have correlated noise at the receiver, two new FTN receivers are proposed. The orthogonalized receiver uses a single filter not matched to the transmitting pulse, but rather one of the basis functions of the pulse. In this sense it is able to "orthogonalize" the received signal by filtering with respect to a new basis. It was discovered that this receiver performs as well as the traditional FTN receiver in terms of capacity. Also proposed was the undersampled receiver architecture. The undersampled architecture attempts to use a standard Nyquist rate receiver to detect an FTN signal. With channel state knowledge known only at the transmitter, this receiver actually performs worse than a Nyquist rate system. However, both the proposed receivers have uncorrelated noise at the receiver. This means that channel capacity for a precoded system with channel state information at the transmitter can be evaluated via the water filling algorithm. It was observed that CSIT improves the capacity of the orthogonalized receiver at low SNRs, but converges to the CSIR capacity as SNR increases. An itemized list of contributions is as follows:

- System description and capacity derivation for a combined FTN MIMO system
- System description and capacity simulation of an orthogonalized FTN receiver
- System description and capacity simulation of a undersampled FTN receiver
- Capacity results with CSIT for the orthogonalized receiver

Designing a System

The research presented in this thesis also provides a framework to design and realize an FTN MIMO system. Block diagrams have been provided for the transmitter and three proposed receivers. Implementation of the receiver's demodulation and decoding systems would ideally be performed on an FPGA. This would allow for efficient implementation of matched filters and the decoder. Ideally the analog components would be kept to a minimum to allow for flexibility in receiver configuration. This means that only the antennas, low noise amplifiers, and possibly a super heterodyne demodulator would be implemented as analog circuits. The same design principle would apply to the transmitter. The power amplifiers and each antenna would ultimately be analog, but the logic to precode, modulate, and sum the appropriate bit streams could be implemented on an FPGA or DSP. Designing such a system would also enable future research in this area.

Future Research

The research performed in this thesis leads to many interesting questions that will become future areas of research. Of primary interest is why the capacities of the orthogonalized FTN receiver and the traditional receiver are so similar. Are they equal and can it be proven? Also of interest is the derivation of a scheme to precode for a traditional FTN receiver with correlated noise. Furthermore, is there a way to relate the system capacity to the Mazo limit of the modulating pulse?

Another large topic is the generalization of the orthogonalized receiver. Currently the architecture only supports rectangular pulses, but the extension to all time limited

pulses and perhaps any general pulse shape would provide further insight into the suspected capacity equality of the orthogonalized and traditional receivers.

Asynchronous transmission of FTN and MIMO data streams is also of interest. All the systems analyzed in this thesis spaced the transmitted streams equally. Is it possible for certain pulse shapes that the optimal delay between streams is a non-equal spacing? Furthermore, if the transmitter is incapable of maintaining synchronization between the streams, how will it affect the system capacity?

The development of a receiver capable of violating the Nyquist rate by amounts other than an integer rate is also interesting. Can a general receiver architecture be realized for any possible FTN rate and can the capacity be derived? More importantly can it be generalized for all pulse shapes, both time limited and band limited.

Of course questions about the architectures derived in this paper still exist. What error correcting code will allow these systems to achieve their Shannon capacity? Can a trellis be designed that will allow for low complexity signal decoding? What will the bit error rate curves of these systems look like? Most importantly, can these systems be constructed and will their actual performance match the theory?

References

[1] M. Yuhas, Y. Feng and J. Bajcsy, "On the Capacity of Faster-than-Nyquist MIMO Transmission with CSI at the Receiver," in *Proc. 2015 IEEE Globecom Workshops (GC Wkshps)*, San Diego, CA, 2015, pp. 1-6.

[2] Wi-Fi Alliance, "15 Years of Wi-Fi," 2015. [Available online].

[3] W. Lehr and L. W. McKnight, "Wireless Internet Access: 3G vs. WiFi?" Aug. 23, 2002.

[4] "The Bluetooth Wireless Technology White Paper," Atmel Corp., San Jose, CA, 2000.

[5] B. A. Black, P. S. DiPiazza, B. A. Ferguson, D. R. Voltmer, and F. C. Berry, *Introduction to Wireless Systems*, Prentice Hall, 2008.

[6] "Realistic LTE Performance from Peak Rate to Subscriber Experience," Motorola, Schaumburg, IL, 2009

[7] M. Habeeb, "QAM is Rising, 1024QAM and Beyond," *Microwaves & RF Mag.*, April 2014.

[8] R. E. Hattachi, J. Erfanian, "5G White Paper," NGMN Alliance, Frankfurt, Germany, 17 February 2015.

[9] F. Boccardi, R. W. Heath Jr., A. Lozano, T. L. Marzetta and P. Popovski, "Five Disruptive Technology Directions for 5G," *IEEE Communications Magazine*, vol. 52, no. 2, pp. 74-80, February 2014.

[10] J.F. Monserrat, et al. “Rethinking the Mobile and Wireless Network Architecture: The METIS Research into 5G,” in *Proc. European Conference on Networks and Communications*, pp. 1-5, Bologna, Italy, June 2014.

[11] A. Osseiran, F. Boccardi, V. Braun, K. Kusume, P. Marsch, M. Maternia, O. Oueseth, M. Schellmann, H. Schotten, H. Taoka, H. Tullberg, M.A. Uusitalo, B. Timus, M. Fallgren, “Scenarios for 5G Mobile and Wireless Communications: The Vision of the METIS Project,” *IEEE Communication Magazine*, vol. 52, no. 5, pp. 26-35, May 2014.

[12] I. Darwazeh, T. Xu, T. Gui, Y. Bao, Z. Li, “Optical SEFDM System: Bandwidth Saving Using Non-orthogonal Sub-Carriers,” *IEEE Photonic Technology Letters*, vol. 26, no. 4, pp. 352-355, Dec. 2013.

[13] Y. Saito, Y. Kishiyama, A. Benjebbour, T. Nakamura, A. Li, K. Higuchi, “Non-Orthogonal Multiple Access (NOMA) for Cellular Future Radio Access,” in *Proc. IEEE 77th Vehicular Technology Conference*, pp. 1-5, Dresden, Germany, June 2013.

[14] M. El Hefnawy, H. Taoka, “Overview of Faster-Than-Nyquist for Future Mobile Communication Systems,” in *Proc. 77th IEEE Vehicular Technology Conference*, pp. 1-5, Dresden, Germany, June 2013.

[15] J.B. Anderson, F. Rusek, V. Öwall, “Faster-than-Nyquist Signaling,” *Proceedings of the IEEE*, vol. 101, no. 8, pp. 1817-1830, March 2013.

[16] A. Modenimi, F. Rusek, G. Colavolpe, “Optimal Transmit Filters for ISI Channels under Channel Shortening Detection,” *IEEE Transactions on Communications*, vol. 61, no. 12, pp. 4997-5005, December 2013.

[17] Y.J. Kim, J. Bajcsy, “Information Rates of Cyclostationary Faster-than-Nyquist Signaling,” in *Proc. IEEE 12th Canadian Workshop on Information Theory*, pp. 1-4, Kelowna, BC, May 2011.

[18] Y.J. Kim, J. Bajcsy, “Iterative Receiver for Faster-than-Nyquist Broadcasting,” *Electronics Letters*, vol. 48, no. 24, pp. 1561-1562 November 2012.

[19] D. Rainnie, Y. Feng and J. Bajcsy, "On capacity merits of spectrally efficient FDM," *Military Communications Conference, MILCOM 2015 - 2015 IEEE*, Tampa, FL, 2015, pp. 581-586.

[20] Huawei Marine Networks, “Tata Communications, Huawei and Huawei Marine Complete First 400G Long-Haul Subsea Network Field Trial,” May 2014. [Available online]

[21] A. Goldsmith, “Multiple Antennas and Space-Time Communications,” in *Wireless Communications*, Cambridge University Press, 2005.

[22] I.E. Telatar, “Capacity of Multiple-antenna Gaussian Channels,” *European Transactions on Telecommunications*, vol. 10, no. 6, pp. 585-595, November-December 1999.

[23] L. Zheng and D.N.C. Tse, “Diversity and Multiplexing: A Fundamental Tradeoff in Multiple-Antenna Channels,” in *IEEE Transactions on Information Theory*, vol. 49, no. 5, pp. 1073-1096, May 2003.

[24] F. Rusek, “On the Existence of the Mazo-Limit on MIMO Channels,” *IEEE Transactions on Wireless Communications*, vol. 8, no. 3, pp. 1118-1121, March 2009.

[25] F. Rusek, “A First Encounter with Faster-than-Nyquist Signaling on the MIMO Channel,” in *Proc. IEEE Wireless Communications and Networking Conference*, pp. 1093-1097, Kowloon, March 2007.

[26] A. Goldsmith, S. A. Jafar, N. Jindal and S. Vishwanath, "Capacity limits of MIMO channels," in *IEEE Journal on Selected Areas in Communications*, vol. 21, no. 5, pp. 684-702, June 2003.

[27] N. Mysore, “Turbo-coded MIMO Systems: Receiver Design and Performance Analysis,” PhD thesis, EECS, McGill University, Montréal, QC, 2006.

[28] T.M. Cover, J.A. Thomas, *Elements of Information Theory*, Wiley Interscience, July 2006.

[29] Y.J. Kim, “Faster than Nyquist Transmission over Continuous-Time Channels: Capacity Analysis and Coding,” PhD thesis, EECS, McGill University, Montréal, QC, 2013.